BMP signaling regulates satellite cell dependent postnatal muscle growth

Stantzou, A., Schirwis, E., Swist, S., Alonso-Martin, S., Polydorou, I., Zarrouki, F., Mouisel, E., Beley, C., Julien, A., Le Grand, F., Garcia, L., Colnot, C., Birchmeier, C., Braun, T., Schuelke, M., Relaix, F., Amthor, H.

Development
2017 AUG 01 ; 144(15): 2737-2747
doi: 10.1242/dev.144089
Publisher: The Company of Biologists Ltd

© 2017. Published by The Company of Biologists Ltd | Development (2017) 144, 2737-2747 doi:10.1242/dev.144089

BMP signaling regulates satellite cell-dependent postnatal muscle growth

Amalia Stantzou[1,2,3], Elija Schirwis[1,3,4], Sandra Swist[5,6], Sonia Alonso-Martin[3,7], Ioanna Polydorou[1,2], Faouzi Zarrouki[1], Etienne Mouisel[3,8], Cyriaque Beley[9], Anaïs Julien[10], Fabien Le Grand[3], Luis Garcia[1], Céline Colnot[10], Carmen Birchmeier[4], Thomas Braun[5], Markus Schuelke[2], Frédéric Relaix[3,7] and Helge Amthor[1,11,*]

ABSTRACT

Postnatal growth of skeletal muscle largely depends on the expansion and differentiation of resident stem cells, the so-called satellite cells. Here, we demonstrate that postnatal satellite cells express components of the bone morphogenetic protein (BMP) signaling machinery. Overexpression of noggin in postnatal mice (to antagonize BMP ligands), satellite cell-specific knockout of *Alk3* (the gene encoding the BMP transmembrane receptor) or overexpression of inhibitory SMAD6 decreased satellite cell proliferation and accretion during myofiber growth, and ultimately retarded muscle growth. Moreover, reduced BMP signaling diminished the adult satellite cell pool. Abrogation of BMP signaling in satellite cell-derived primary myoblasts strongly diminished cell proliferation and upregulated the expression of cell cycle inhibitors *p21* and *p57*. In conclusion, these results show that BMP signaling defines postnatal muscle development by regulating satellite cell-dependent myofiber growth and the generation of the adult muscle stem cell pool.

KEY WORDS: BMP signaling, Postnatal muscle growth, Satellite cells, Muscle stem cells, Mouse

INTRODUCTION

The basic cellular units of skeletal muscle are myofibers, which are multinuclear syncytia capable of contraction. Myofibers, which are generated during prenatal development, continue to grow after birth (White et al., 2010). This postnatal growth requires a sufficiently large pool of muscle precursors, the so-called satellite cells, which reside between the basal lamina and the sarcolemma of muscle fibers (Mauro, 1961). During the first 3 weeks of postnatal mouse development, muscle fibers grow through the recruitment of satellite cells (accretion), thereby enlarging the number of myonuclei, as well as expanding the cytoplasmic domain. Thereafter, muscle fibers grow mainly by expanding their cytoplasmic volume without further addition of myonuclei (White et al., 2010). Whereas postnatal satellite cells cycle to generate progenitors for fusion with the muscle fibers, they are quiescent in adult muscle and are only reactivated for the regeneration of damaged muscle fibers (Beilharz et al., 1992). The postnatal growth period is accompanied by a steady decline in the number of muscle satellite cells until 21 days after birth and remains stable thereafter throughout adulthood (White et al., 2010).

Little is known about the intercellular signaling systems that guide postnatal muscle growth and determine adult satellite cell number. We and others have previously described the crucial role of bone morphogenetic proteins (BMPs) during embryonic, fetal and adult muscle growth (Amthor et al., 1998, 1999, 2002; Hirsinger et al., 1997; Ono et al., 2011; Pourquié et al., 1996; Sartori et al., 2013; Wang et al., 2010). In parallel with other members of the TGFβ family of signaling molecules, BMPs act on target cells via transmembrane serine/threonine kinase receptors. BMPs bind to type II and type I receptors, and form a ligand-receptor complex that permits the phosphorylation of the type I receptor via the constitutively active type II receptor (Nohe et al., 2004, 2002). The type I receptor in turn phosphorylates the BMP-responsive Smad1/5/8 proteins. Phosphorylated Smad1/5/8 proteins subsequently form complexes with co-Smad4 and translocate into the nucleus to regulate transcriptional activity of target genes such as DNA-binding protein inhibitors (*Ids*) (Miyazono and Miyazawa, 2002). Four isoforms of these proteins (Id1-4) block the binding of E proteins with the myogenic regulatory transcription factor MyoD and inhibit terminal differentiation (Jen et al., 1992). Interestingly, BMP signaling upregulates the inhibitory *Smad6* as part of a negative feedback loop. Smad6 interferes with BMP signaling at the level of the receptor, as well as at the level of the complex formation between receptor-regulated Smad1 and the common mediator co-Smad4 (Goto et al., 2007).

A number of secreted proteins, such as noggin (Nog), can non-covalently bind BMPs, thereby impeding their receptor binding (Amthor et al., 2002; Krause et al., 2011). The BMP/Nog antagonism regulates satellite cell lineage progression. We have previously demonstrated *in vitro* that BMP signaling stimulated proliferation of activated adult satellite cells and inhibited myogenic differentiation, whereas abrogation of BMP signaling via addition of Nog, induced precocious differentiation (Ono et al., 2011). Interestingly, myotube formation is delayed in *Nog*-null mice, pointing to a requirement for Nog expression for proper muscle differentiation (Tylzanowski et al., 2006). Moreover, injection of Nog into regenerating muscle inhibited BMP signaling and reduced P-Smad1/5/8, Id1 and Id3 protein levels (Clever et al., 2010).

[1]Versailles Saint-Quentin-en-Yvelines University, INSERM U1179, LIA BAHN CSM, Montigny-le-Bretonneux 78180, France. [2]Department of Neuropediatrics and NeuroCure Clinical Research Center, Charité University-Medicine, Berlin 10117, Germany. [3]Pierre et Marie Curie University, Paris Sorbonne, INSERM, UMRS974, CNRS FRE3617, Center for Research in Myology, Paris 75013, France. [4]Developmental Biology/Signal Transduction Group, Max Delbruck Center for Molecular Medicine, Berlin 13092, Germany. [5]Department of Cardiac Development and Remodeling, Max-Planck-Institute for Heart and Lung Research, Bad Nauheim 61231, Germany. [6]Department of Cardiovascular Physiology, Ruhr University Bochum, D-44780 Bochum, Germany. [7]INSERM, Paris Est University, IMRB U955-E10, Créteil 94010, France. [8]Paul Sabatier University, Inserm UMR 1048, Toulouse 31432, France. [9]SQY Therapeutics, Montigny-le-Bretonneux 78180, France. [10]Paris Descartes-Sorbonne Paris Cité University, Inserm UMR1163, Imagine Institute, Paris 75015, France. [11]Pediatric Department, University Hospital Raymond Poincaré, Garches 92380, France.

*Author for correspondence (helge.amthor@uvsq.fr)

S.A., 0000-0002-3254-0365; F.R., 0000-0003-1270-1472; H.A., 0000-0003-1008-719X

Received 30 August 2016; Accepted 21 June 2017

Development (2017) 144, 2737-2747 doi:10.1242/dev.144089

Based on our previous *in vitro* findings (Ono et al., 2011), we set out to determine the role of BMP signaling on satellite cells *in vivo*. We chose the early postnatal/juvenile growth phase of mouse limb muscles as our main experimental model because satellite cell activation, proliferation and differentiation, as well as fiber growth, can be much more easily observed when compared with regeneration models. We used three independent techniques to interfere with BMP signaling in satellite cells: (1) addition of Nog, which interferes at the ligand level; (2) abrogation of the BMP transmembrane receptor *Alk3*, which interferes at the receptor level; and (3) overexpression of *SMAD6*, which interferes with BMP signaling at the cell-autonomous level. We show that abrogation of BMP signaling severely inhibits satellite cell activity, myonuclear recruitment and the generation of the adult satellite cell pool.

RESULTS

BMP signaling is active in postnatal muscle satellite cells

We first asked whether the BMP signaling pathway is active during the postnatal growth phase of skeletal muscle. We found the presence of transcripts of genes encoding different BMP ligands, the BMP receptor Alk3 (also known as *Bmpr1a*), the BMP target gene *Id1* (Miyazono and Miyazawa, 2002), as well as the BMP antagonists *Nog*, *Grem1*, *Fst* and *Chrd* (respectively encoding for Nog, gremlin 1, follistatin and chordin) in total RNA extracted from limb skeletal muscle of 3- ,14-, 21- and 28-day-old mice (Fig. S1A). Generally, the mRNA concentrations for BMP signaling components declined from postnatal to young adult stages.

In order to identify whether satellite cells respond to BMP signaling, we monitored the nuclear accumulation of BMP-induced Smad1/5 proteins in Pax7-positive nuclei using double immunohistochemistry. We discovered P-Smad1/5-positive and -negative satellite cells in postnatal, juvenile and young adult muscle (from 3-, 14-, 21- and 28-day-old mice) (Fig. 1). We also found P-Smad1/5-positive nuclei that were negative for Pax7, which mainly were myonuclei within myofibers, as judged from their position.

We next examined the time frame and dynamics of the response of satellite cells to BMPs. For this, satellite cells were isolated from 6- to 8-week-old mice by magnetic-activated cell sorting (MACS) and expanded in culture, which maintained Pax7 expression in nearly 100% of cells in all the described conditions. Cells were then submitted to a serum-free culture condition supplemented with soluble Alk3 receptor for 6 h, thereby removing residual BMP ligands otherwise likely present in the culture medium. Thereafter, culture medium was replaced with serum-free medium containing 100 ng/ml of BMP4 for 1 h, which increased nuclear levels of phosphorylated Smad1/5 protein in the cells (Fig. S1B,C), clearly indicating that they respond to BMP signaling. Additionally, by performing a time course study, we found that *Id1* mRNA copy numbers peaked 1 h after BMP4 exposure and slowly declined thereafter (Fig. S1D). Interestingly, in control cultures, *Id1* expression increased slowly following medium change from Alk3 pre-treatment to vehicle supplemented control medium (not containing Alk3), suggesting that cells synthesize BMPs and therefore respond to BMP signaling in an autocrine/paracrine fashion. This hypothesis was further supported by the finding that *Id1* mRNA copy numbers in serum-deprived control cells could be further halved through addition of sAlk3, which sequestered the satellite cell-derived BMPs.

Having found that satellite cells activate the BMP signaling cascade, we next studied the expression of BMP signaling components in FACS-isolated muscle satellite cells from 3-, 14-,

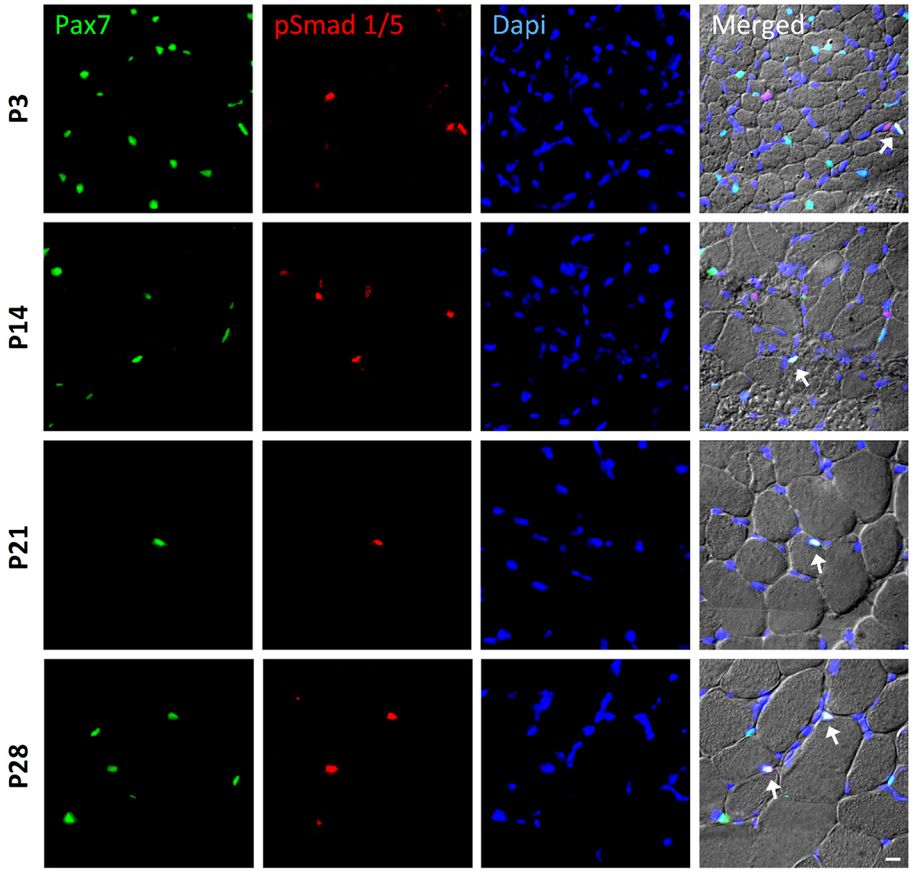

Fig. 1. BMP signaling activity in satellite cells during postnatal muscle growth. Sample images of immunohistochemistry to monitor phosphorylated Smad1/5 (p-Smad1/5) expression (red) in Pax7-expressing satellite cells (green). Muscle sections were obtained from the tibialis anterior (TA) muscle of postnatal wild-type mice at P3, P14, P21 and P28 (panels from top to bottom). DAPI (blue) was used as a nuclear stain. All three channels (green, red and blue) were merged together with a differential interference contrast image (DIC), in which the individual fibers can be visualized. Cells that co-express p-Smad1/5 and Pax7 are highlighted with arrows. Scale bar: 50 µm.

Development (2017) 144, 2737-2747 doi:10.1242/dev.144089

21- and 28-day-old mice. We found that satellite cells expressed transcripts of all BMP signaling components, as demonstrated above for whole-muscle extracts with the exception of only *Bmp14* (Fig. 2). Interestingly, mRNA expression levels were generally more than 10 times higher in satellite cells than in total muscle extracts (Fig. S1A). In total muscle extracts, the decline of satellite cell-specific gene expression signatures with muscle maturation towards day P21 can well be explained by a dilution effect due to the overall reduction of satellite cell number by 65% between days P6 and P21 (White et al., 2010). Expression levels of several genes encoding BMP signaling components in satellite cells, such as *Alk3*, *Id1* and *Nog*, transiently decreased at P14, whereas expression of others decreased from postnatal to adult stages or remained steady (Fig. 2). Among the different analyzed BMP ligands, *Bmp6* was most strongly expressed and expression peaked in adult satellite cells. These results suggest that BMP signaling plays a role during satellite cell-dependent postnatal muscle growth; however, there is no general rule in their expression dynamics during muscle maturation.

The BMP antagonist Nog retards postnatal satellite cell-dependent muscle growth

We next interrupted the BMP signaling cascade during postnatal muscle growth *in vivo* and ectopically overexpressed the BMP antagonist Nog by transfecting the whole muscle using an AAV-expressing vector. Tibialis anterior (TA) and triceps brachii (TB) muscles were transfected at P3 with an AAV-*Nog*, which resulted in high transgene expression (Fig. S2A). We have previously shown that AAV strongly transfects differentiated muscle fibers. However, as Nog is a secreted protein it would accumulate in the extracellular space. Nog overexpression significantly retarded muscle growth when compared with saline injected controls, which could be verified by anatomical analysis of skeletal muscle at 4 weeks of age (Fig. 3A). The muscle weight of Nog-treated muscles was considerably smaller than the weight of control limbs (Fig. 3B). Indeed, TB, TA and EDL (extensor digitorum longus) muscle weights were reduced by 15%, 21% and 23%, respectively. Morphometric analysis of single fibers or of transverse sections from TA muscles revealed a strong shift of myofiber diameters towards smaller fiber sizes (Fig. 3C and Fig. S2B,E), whereas fiber length remained unchanged (Fig. S2C), which is evidence for postnatal fiber growth retardation. Postnatal skeletal muscle enlarges via continuous recruitment of satellite cells into the growing myofiber syncytium. Hence, the total number of myonuclei in one fiber reflects the cumulative history of previous satellite cell activity. In order to understand the cellular mechanism that results in Nog-induced growth retardation, we determined the total number of myonuclei on isolated muscle fibers from TA muscles prior to and after Nog overexpression. Prior to Nog transfection at day P3, muscle fibers contained 74±2 myonuclei, which increased in control muscles to 419±11 myonuclei, whereas Nog-treated myofibers increased the number of their myonuclei to only 244±5 (mean±s.e.m.) (Fig. 3D and Fig. S2D). Thus, whereas the number of myonuclei increased by 5.7-fold between days P3 and P28 in controls, the presence of Nog reduced the increase to 3.3-fold, indicating that satellite cell function during postnatal myofiber growth might be impaired.

The BMP antagonist Nog decreases postnatal satellite cell activity

We next studied the effect of Nog on satellite cell proliferation during the postnatal growth phase. We treated mice at P3 with AAV-*Nog*, administered BrdU at P14 for 3 consecutive days and analyzed muscles at P17. The state of the muscle precursor cells was subsequently determined using anti-Pax7 and anti-BrdU immunostaining: $Pax7^{+}/BrdU^{+}$ marking proliferating satellite cells, $Pax7^{+}/BrdU^{-}$ marking quiescent satellite cells and $Pax7^{-}/BrdU^{+}$ with subsarcolemmal position marking former satellite cells that had divided and differentiated to become mitotically inactive once recruited into the myofiber (Fig. 4A). Interestingly, we found that the total number of $Pax7^{+}$ cells was reduced after Nog-mediated

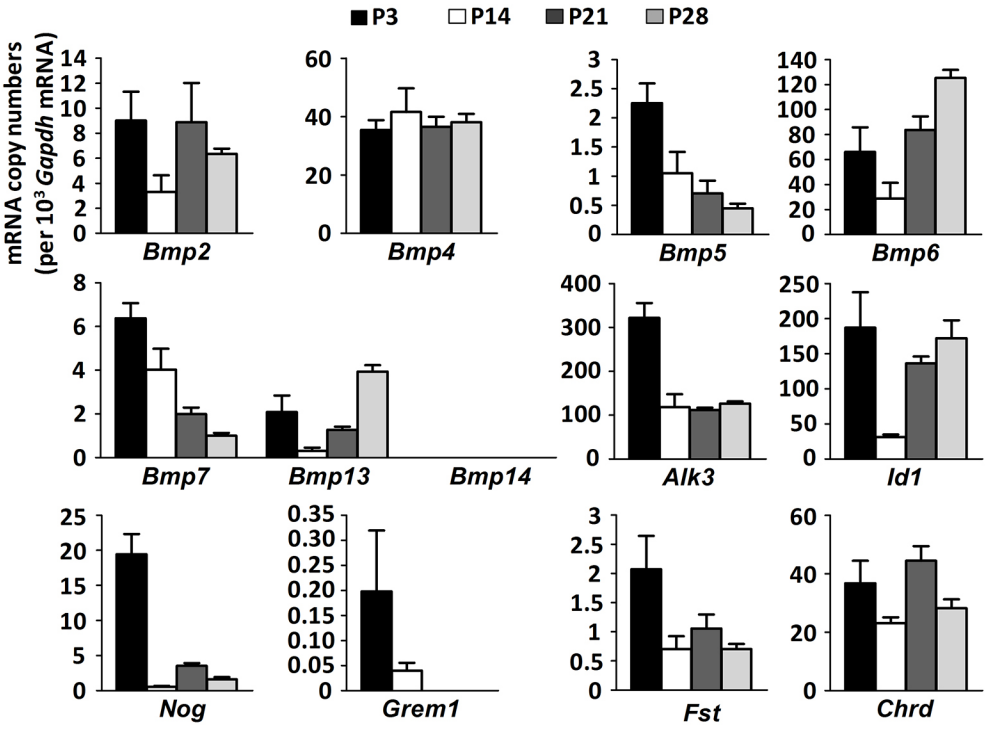

Fig. 2. Expression dynamics of BMP signaling pathway components in satellite cells during postnatal muscle growth. The relative mRNA copy numbers per 10^3 *Gapdh* mRNA copies of different BMP ligands (*Bmp2*, *Bmp4*, *Bmp5*, *Bmp6*, *Bmp7*, *Bmp13* and *Bmp14*), BMP receptor type I *Alk3*, BMP target gene *Id1*, BMP antagonists *Nog* (encoding Noggin), *Grem1* (encoding gremlin), *Fst* (encoding follistatin) and *Chrd* (encoding chordin) in satellite cells that were isolated by FACS from skeletal muscles of wild-type mice (*n*=3 biological and technical replicates) at P3, P14, P21 and P28. Data are mean±s.e.m.

Development (2017) 144, 2737-2747 doi:10.1242/dev.144089

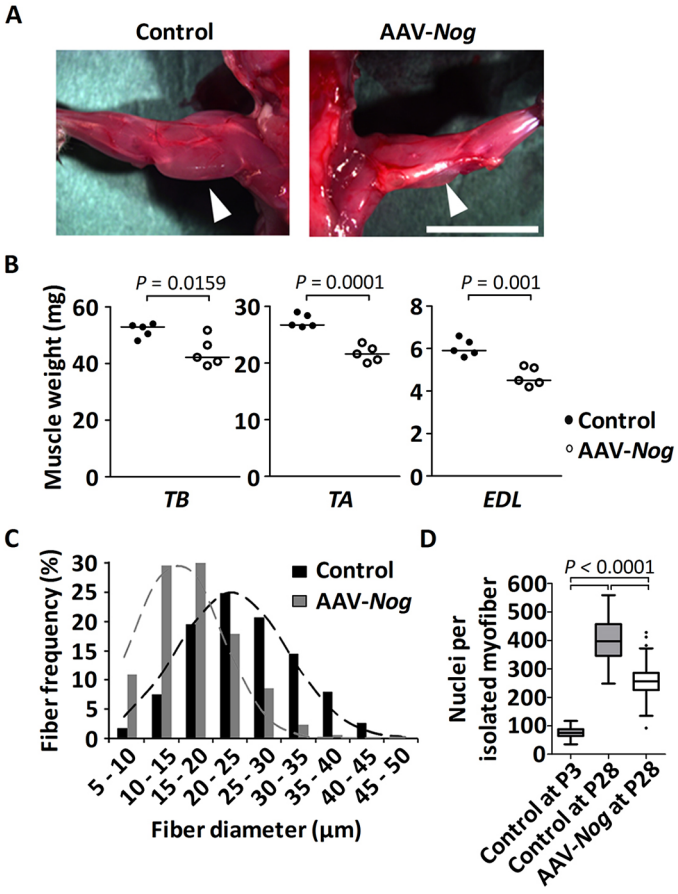

Fig. 3. Consequences of Nog-mediated abrogation of BMP signaling for postnatal muscle growth. Triceps brachii (TB) muscle and the anterior compartment of the lower hindlimb were transduced with AAV-*Nog* at P3. Muscles were analyzed at 4 weeks of age. (A) Dorsal view of the forelimb shows significant muscle hypotrophy (arrowheads) of the AAV-*Nog*-treated TB muscle (right) when compared with the control saline-injected contralateral side (left). Sample images of n=4 injected mice. Scale bar: 1 cm. (B) Dot plots depict muscle wet weight of TB, TA and EDL muscles. Horizontal lines represent the median. (C) Histogram of the fiber diameters of 4-week-old TA muscle, analyzed on mid-belly muscle sections following immunostaining against laminin. Dashed lines represent the fitted normal distribution. (D) The number of myonuclei per single fiber of the TA muscle at P3 (n=50 fibers from 3 mice) and at P28 following AAV-*Nog* (n=120 fibers from 3 mice) or saline (n=68 fibers from 3 mice) injections at P3. Data are depicted as Whiskers-Tukey box plots. Boxes indicate the interquartile range (IQR), the horizontal line indicates the median, whiskers indicate [1.5 × IQR] and dots indicate the outliers.

abrogation of BMP signaling (Fig. 4B). Moreover, all three Pax7$^+$/BrdU$^+$, Pax7$^+$/BrdU$^-$ and Pax7$^-$/BrdU$^+$ cell populations were reduced after AAV-*Nog* treatment (Fig. 4B). Decreased satellite cell proliferation was thus the main cellular mechanism that caused reduced myonuclear recruitment and reduced postnatal muscle growth. Indeed, the precocious differentiation of satellite cells would be unlikely, as the number of newly formed myonuclei was reduced. Moreover, the reduction of the Pax7$^+$/BrdU$^-$ population suggested a decrease of satellite cell self-renewal and thus a decline of the satellite cell pool in states of abrogated BMP signaling.

At about 21 days of age, the final satellite cell number is established and does not further increase towards adulthood (White et al., 2010). We therefore wanted to investigate the consequence of this decreased satellite cell proliferation during the postnatal stages for the generation of the adult muscle stem cell pool. Remarkably, treatment with Nog at day P3 decreased the reservoir of satellite cells at 4 weeks of age to about half the size of controls when counting Pax7$^+$ and cadherin$^+$ cells (Fig. 4C,D and Fig. S2E). In summary, these findings demonstrate that adult muscle stem cells are generated during the postnatal growth phase under the control of BMP signaling.

Conditional Alk3 knockout results in reduced postnatal muscle growth and a reduced satellite cell reservoir

In order to evaluate the role of BMP signaling in activated satellite cells during postnatal muscle growth more specifically, we tested the consequence of cell-autonomous abrogation of the BMP signaling pathway by ablating *Alk3*, the BMP type I receptor, exclusively in postnatal Pax7-expressing satellite cells. This aim was achieved by generating *Pax7*$^{CreERT2/+}$;*Alk3*$^{flox/flox}$ mice and inducing the *Alk3* knockout by administering tamoxifen at postnatal days P7 and P9. We analyzed the effect of *Alk3* knockout on muscle growth at 4 weeks of age in comparison with genetic controls (tamoxifen injected *Alk3*$^{flox/flox}$ mice). Tamoxifen treatment of *Pax7*$^{CreERT2/+}$;*Alk3*$^{flox/flox}$ pups resulted, just like Nog treatment, in muscle fiber hypotrophy. Indeed, morphometric fiber size analysis of transverse cross-sections from TA muscles revealed a shift towards smaller fiber sizes (Fig. 5A,B). Similar to the Nog treatment, isolated EDL myofibers from tamoxifen-treated 4-week-old *Pax7*$^{CreERT2/+}$;*Alk3*$^{flox/flox}$ mice contained significantly fewer myonuclei than their respective controls (Fig. 5C). Furthermore, the number of Pax7$^+$ satellite cells was also decreased in tamoxifen-treated *Pax7*$^{CreERT2/+}$;*Alk3*$^{flox/flox}$ mice when compared with controls (Fig. 5D).

Overexpression of *SMAD6* inhibits satellite cell-dependent postnatal muscle growth and the generation of the adult satellite cell pool

We additionally tested a different means for cell-autonomous abrogation of BMP signaling during postnatal muscle growth via overexpression of *SMAD6*, an inhibitory Smad of the intracellular BMP signaling cascade, specifically in Pax7-expressing satellite cells. Such time- and lineage-specific expression of *SMAD6* was achieved by crossing *Pax7*$^{CreERT2/+}$ mice with *Rosa26*$^{Lox\text{-}Stop\text{-}Lox\text{-}huSMAD6\text{-}IRES\text{-}EGFP}$ (*RS6*) mice and subsequent activation of the transgene by tamoxifen through removal of a stop codon. *SMAD6* mRNA expression, taken as evidence for successful Cre-induced recombination (Fig. S2F), was found only in satellite cell-derived myoblasts from tamoxifen-treated *Pax7*$^{CreERT2/+}$;*RS6*$^{+/-}$ mice, but not from control mice. We administered tamoxifen to *Pax7*$^{CreERT2/+}$;*RS6*$^{+/-}$ mice at P7 and P9, and analyzed the effect on muscle growth at 4 weeks of age in comparison with genetic controls (tamoxifen-treated *RS6*$^{+/-}$ mice), thus using the same experimental protocol as for the *Alk3* knockout. Tamoxifen treatment of *Pax7*$^{CreERT2/+}$;*RS6*$^{+/-}$ pups resulted in muscle fiber hypotrophy, similar to Nog treatment and *Alk3* knockout. Indeed, morphometric fiber size analysis of transverse cross-sections from TA muscles revealed a shift towards smaller fiber sizes in tamoxifen-treated *Pax7*$^{CreERT2/+}$;*RS6*$^{+/-}$ mice when compared with controls, indicating that the decrease of muscle growth results from a failure to increase the myofiber size (Fig. 6A, B). Importantly, this failure of muscle fiber growth was not compensated for during later development. Indeed, myofibers were still smaller in 2-month-old tamoxifen-treated *Pax7*$^{CreERT2/+}$;*RS6*$^{+/-}$ mice when compared with controls (Fig. S2G-I). Moreover, isolated EDL myofibers from tamoxifen-treated, 4-week-old *Pax7*$^{CreERT2/+}$;*RS6*$^{+/-}$ mice contained fewer myonuclei than their respective controls (Fig. 6C), whereas the myonuclear domain of the

Development (2017) 144, 2737-2747 doi:10.1242/dev.144089

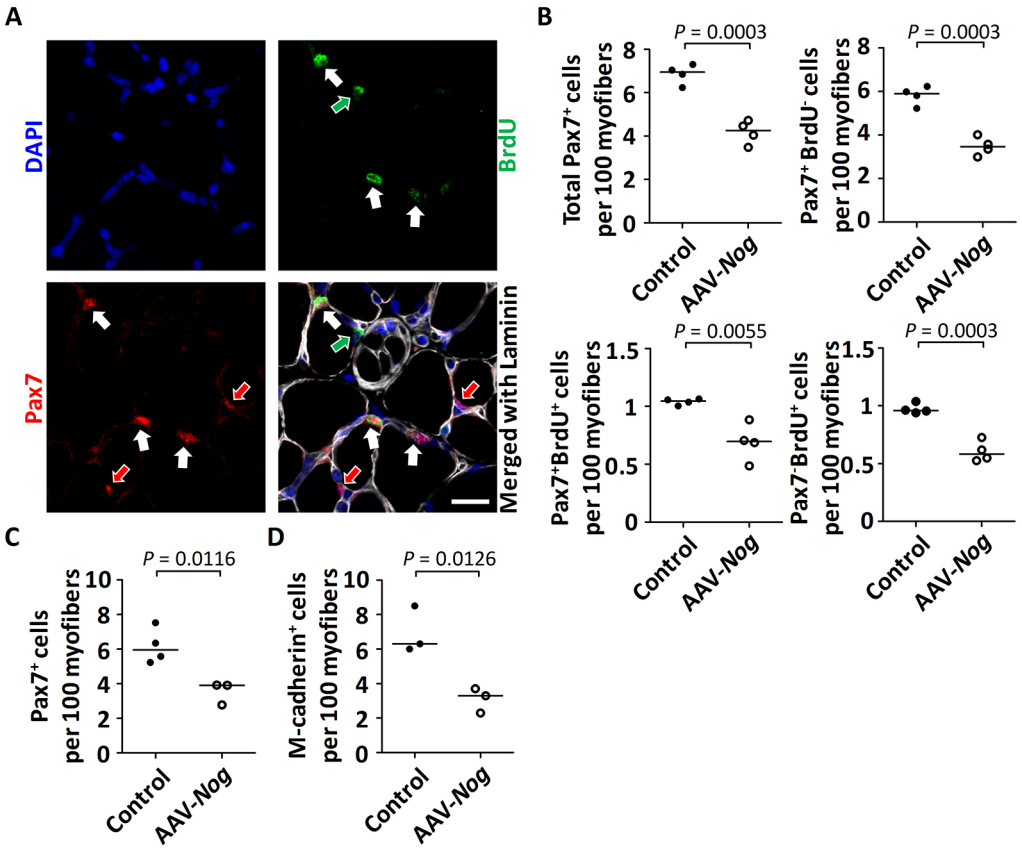

Fig. 4. Effects of Nog-mediated abrogation of BMP signaling on postnatal satellite cell activity. The anterior compartment of the lower hindlimb was transduced with AAV-*Nog* at P3. At P14, the mice were treated for 3 consecutive days with subcutaneous injections of BrdU and were sacrificed at P17. (A) Fluorescence images of a mid-belly transverse section of a TA muscle following immunostaining against Pax7 in red (arrows), against BrdU (green) and against laminin (white); nuclei were stained with DAPI (blue). $Pax7^+/BrdU^+$ cells are indicated with white arrows. $Pax7^+/BrdU^-$ satellite cells and $Pax7^-/BrdU^+$ sublaminal myonuclei are, respectively, indicated with red and green arrows. Scale bar: 20 µm. (B) The diagrams depict the number of $Pax7^+$, $Pax7^+BrdU^-$ and $Pax7^+BrdU^+$ satellite cells, as well as the number of newly recruited $Pax7^-BrdU^+$ myonuclei per 100 myofibers from the TA muscle. *n*=4 biological replicates for each condition. (C,D) The anterior compartment of the lower hindlimb was transduced with AAV-*Nog* at P3. Muscles were analyzed at 4 weeks of age. The diagram depicts the number of $Pax7^+$ (C) and of m-$Cadherin^+$ (D) satellite cells per 100 myofibers quantified from whole TA muscle sections (*n*=3 or 4 for saline-injected control; *n*=3 for AAV-*Nog*-injected muscle). Horizontal lines represent the median and dots represent individual data points.

fibers remained unchanged (Fig. 6D). These results suggest decreased satellite cell activity during the postnatal muscle growth phase in satellite cells that lack BMP signaling. Indeed, the number of $Pax7^+$ satellite cells, if quantified on both muscle cross-sections or isolated fibers, was decreased in tamoxifen-treated $Pax7^{CreERT2/+};RS6^{+/-}$ mice when compared with controls (Fig. 6E,F). Finally, the satellite cell pool remained decreased by 75% when 8-week-old TA muscles from tamoxifen-treated $Pax7^{CreERT2/+};RS6^{+/-}$ mice were compared with control muscles (Fig. S2J). This can be taken as further evidence that adult satellite cells are generated during the postnatal growth phase under the control of BMP signaling.

Expression of *SMAD6* in myonuclei does not alter satellite cell and myonuclear number

The aforementioned experiments failed to provide unequivocal evidence of whether the *SMAD6*-mediated cell-autonomous inhibition of BMP signaling was the sole cause for the observed decrease in the numbers of satellite cells and myonuclei. As an alternative explanation, the inclusion of *SMAD6*-overexpressing myonuclei may indirectly influence satellite cell activity. Hence, we generated $HSA\text{-}Cre^+;RS6^{+/-}$ mice to overexpress *SMAD6* exclusively in terminally differentiated myofibers. Muscles from these mice expressed *SMAD6* as well as GFP, suggesting the effective recombination of the transgene (Fig. S3A,B). Of note, GFP could be detected only on western blot and not using fluorescence analysis of dissected muscles *in toto* or of sectioned muscle (data not shown). Histological analysis of cross-sections of TA muscles from 4- and 8-week-old $HSA\text{-}Cre^+;RS6^{+/-}$ mice revealed a normal tissue architecture (Fig. S3C). Importantly, the number of $Pax7^+$ satellite cells did not change in 4- and 8-week-old $HSA\text{-}Cre^+;RS6^{+/-}$ mice when compared with controls (Fig. S3D,E). Taken together, these experiments ruled out an indirect effect of *SMAD6*-overexpressing myonuclei on satellite cells and therefore confirm that BMP signaling acts in a cell-autonomous manner in satellite cells.

BMP signaling is required for myoblast activation and proliferation

We next used *in vitro* cell culture to further explore the role of BMP signaling on satellite cell-derived muscle precursor cells. Cultures of FACS-sorted satellite cells from adult forelimb and hindlimb $Pax7^{CreERT2/+};RS6^{+/-}$ muscles were treated either with 1 µM hydroxytamoxifen (4-OHT) to evaluate the cell-autonomous effect of *SMAD6* upregulation or with 50 ng/µl recombinant Nog to antagonize BMP ligands present in the culture medium (Fig. S4A). The 4-OHT-treated cells strongly expressed *SMAD6*, but not the cells from untreated control cultures (Fig. 7A). Furthermore, 4-

Development (2017) 144, 2737-2747 doi:10.1242/dev.144089

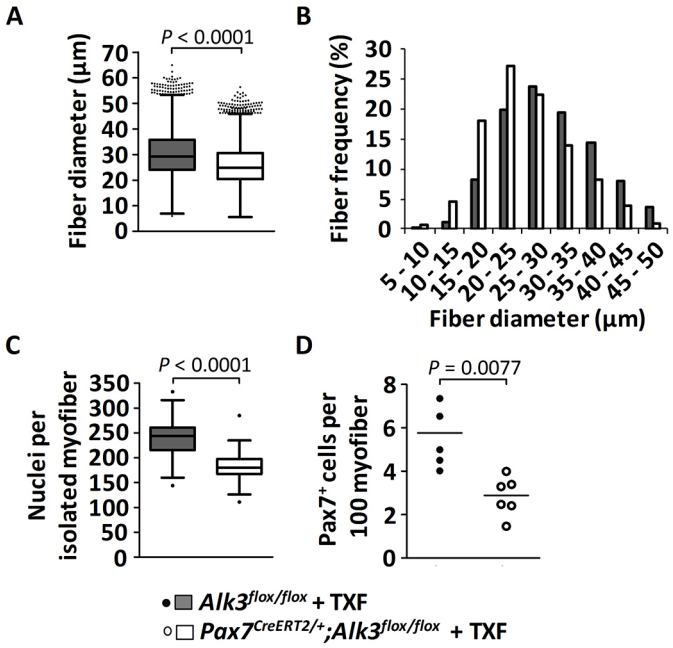

Fig. 5. Consequences of *Alk3* knockout in satellite cells on postnatal muscle growth. Mice were injected with tamoxifen (TXF) at P7 and P9, and sacrificed at the age of 1 month. (A,B) Quantification of the diameter of TA muscle fibers [depicted as Whiskers-Tukey box plots (A) and as a histogram (B)] of mid-belly muscle sections following immunostaining against laminin, from control tamoxifen-treated *Alk3*$^{flox/flox}$ mice (n=4, gray) compared with tamoxifen-treated *Pax7*$^{CreERT2/+}$;*Alk3*$^{flox/flox}$ mice (n=4, white). (C) The Whiskers-Tukey box plots depict the number of myonuclei per isolated muscle fiber from EDL muscles from control tamoxifen-treated *Alk3*$^{flox/flox}$ mice (n=49 fibers from 3 mice) compared with tamoxifen-treated *Pax7*$^{CreERT2/+}$; *Alk3*$^{flox/flox}$ mice (n=77 fibers from 3 mice). Boxes indicate the interquartile range (IQR), the horizontal line indicates the median, whiskers indicate [1.5 × IQR] and dots indicate the outliers. (D) The dot plot (median indicated by the horizontal line) depicts the number of Pax7$^+$ satellite cells per 100 muscle fibers from TA muscles from control tamoxifen-treated *Alk3*$^{flox/flox}$ mice (n=5, black dots) compared with tamoxifen-treated *Pax7*$^{CreERT2/+}$; *Alk3*$^{flox/flox}$ mice (n=6, white dots).

OHT and Nog downregulated the BMP target gene *Id1* (Fig. 7B). These results demonstrate the efficacy of the 4-OHT-induced recombination in *Pax7*$^{CreERT2/+}$;*RS6*$^{+/-}$ satellite cells and the value of Nog as a positive control for abrogation of BMP signaling.

We then assessed cell proliferation by monitoring clonal cell expansion after seeding cells at low density. After 5 days in culture, cells expressed MyoD (Fig. S4B) and lost expression of Pax7 (data not shown), which highlights the transition from satellite cells to committed myoblasts. Both treatment schemes with 4-OHT or with Nog reduced the number of satellite cell-derived myoblast progenitors below 50% of the control values (Fig. 7C). In a control experiment, 4-OHT revealed some inhibiting effect (the number of cells per colony was reduced by 14%) on cell proliferation on its own when treating FACS-isolated *Pax7*$^{CreERT2/+}$ cells. However, this effect was less pronounced than the severe inhibition by Nog or by 4-OHT (the number of cells per colony was reduced by 58% for both treatments) on *Pax7*$^{CreERT2/+}$;*RS6*$^{+/-}$-derived cells (Fig. 7C).

The reduction of cell numbers could not be accounted for by induction of apoptosis because none of the cells under these culture conditions expressed the apoptosis marker cleaved-caspase 3 (data not shown). Furthermore, we found similar proportions of cells expressing myogenin (MyoG) and myosin heavy chain (MHC) in *Pax7*$^{CreERT2/+}$;*RS6*$^{+/-}$-derived cultures treated with 4-OHT and Nog if compared with control cultures (Fig. 7D,E and Fig. S4B-D). This confirmed that the inhibition of BMP signaling does not affect cell lineage progression. Finally, we observed that the number of proliferating Ki67$^+$ cells was decreased by 53% upon treatment with 4-OHT and by 45% with Nog (Fig. 7F and Fig. S4B,E). The decreased proliferation was associated with an increase in transcript levels for the cell cycle inhibitors p57 and p21, suggesting a cell cycle arrest as the likely molecular mechanism following abrogation of BMP signaling (Fig. 7G,H).

DISCUSSION

The present study has provided several important new insights about BMP signaling and its contribution to the regulation of satellite cell-dependent muscle growth in postnatal skeletal muscle. We show that postnatal satellite cells express *in vitro* as well as *in vivo* components of the BMP signaling pathway and respond to BMP signaling. These findings are reminiscent of previous observations on the role of BMP during embryonic and fetal chicken myoblast development and during adult murine satellite cell regulation (Amthor et al., 1998, 1999, 2002; Ono et al., 2011; Wang et al., 2010). We thus conclude that BMP signaling is an important regulator of muscle stem cell activity during all stages of muscle development.

We used AVV-vectors encoding Nog, an efficient antagonist of BMP2, BMP4, BMP5, BMP6, BMP7, BMP13 and BMP14 (all found to be expressed by satellite cells, with the exception of BMP14), as a means to abrogate BMP signaling (Krause et al., 2011). AAV highly transfects muscle fibers following intramuscular injection. Our working hypothesis was that Nog would mainly be synthesized and secreted from muscle fibers, thereby changing the signaling environment, including that of satellite cells by antagonizing locally present BMPs. We do not know whether AAV-Nog also transfected satellite cells. However, as the transgene remains episomal, it does not replicate during cell division and would be rapidly diluted among the muscle cell progenitors. We show that Nog-mediated BMP blockade decreased satellite cell proliferation, which well explains decreased myonuclear accretion during postnatal myofiber growth. However, our *in vivo* experiments using AAV-mediated Nog overexpression could not exclude the possibility of secondary effects on satellite cells, i.e. a change of signaling of the myofiber back to the satellite cells.

We thus used three different inducible Cre-lox systems to either ablate the expression of BMP receptor *Alk3* or to overexpress the BMP intracellular inhibitor *SMAD6* in either satellite cells or differentiated muscle fibers. Both means of cell-autonomous inhibition of BMP signaling (*Alk3* knockout or SMAD6 overexpression) targeted to satellite cells resulted in smaller fibers containing fewer myonuclei and in reduced satellite cell number. We know little about the satellite cell progeny in our loss-of-function models. Our BrdU experiments suggest that satellite cells do not precociously differentiate and that they decline in number because of diminished proliferation. However, direct proof remains missing as the IRES-EGFP cassette of the recombined Smad6 locus in *Pax7*$^{CreERT2/+}$;*RS6*$^{+/-}$ satellite cells was too weakly expressed to allow cell fate tracking. Thus, we cannot exclude other cellular mechanism such as apoptosis.

To address this issue further, we tested loss-of-function strategies *in vitro*. We confirmed diminished proliferation as being responsible for the insufficient progenitor generation. We did not find evidence, either *in vivo* or *in vitro*, of precocious differentiation of myogenic precursors after inhibition of the BMP pathway, which

Development (2017) 144, 2737-2747 doi:10.1242/dev.144089

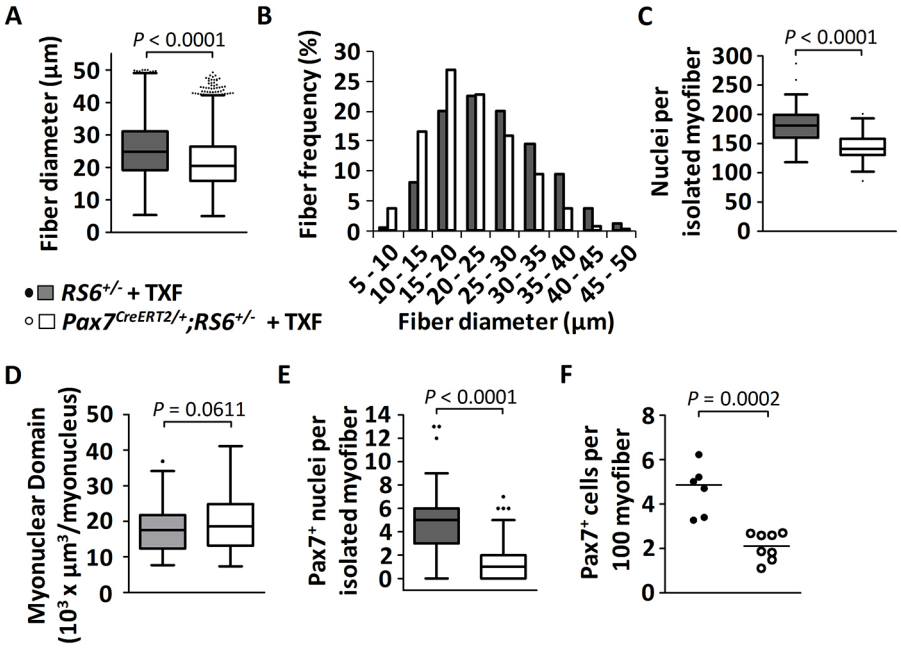

Fig. 6. Consequences of SMAD6-mediated abrogation of BMP signaling in neonatal satellite cells on juvenile muscle growth. Mice were injected with tamoxifen (TXF) at P7 and P9, and sacrificed at the age of 1 month. (A,B) Quantification of the diameter of TA muscle fibers [depicted as Whiskers-Tukey box plots (A) and as a histogram (B)] of mid-belly muscle sections following immunostaining against laminin, from control tamoxifen-treated *RS6*$^{+/-}$ mice (*n*=5, gray) compared with tamoxifen-treated *Pax7*$^{CreERT2/+}$;*RS6*$^{+/-}$ mice (*n*=4, white). (C) The Whiskers-Tukey box plots depict the number of myonuclei per isolated muscle fiber from EDL muscles from control tamoxifen-treated *RS6*$^{+/-}$ mice (*n*=51 isolated fibers from 3 mice) compared with tamoxifen-treated *Pax7*$^{CreERT2/+}$;*RS6*$^{+/-}$ mice (*n*=66 isolated fibers from 4 mice). Boxes indicate the interquartile range (IQR), the horizontal line indicates the median, whiskers indicate [1.5 × IQR] and dots indicate the outliers. (D) The Whiskers-Tukey box plots depict the myonuclear domain analyzed on segments of isolated single fibers from control tamoxifen-treated *RS6*$^{+/-}$ mice (*n*=98 segments from 33 fibers) compared with tamoxifen-treated *Pax7*$^{CreERT2/+}$;*RS6*$^{+/-}$ mice (*n*=182 segments from 61 fibers). (E) The Whiskers-Tukey box plots depict the number of Pax7^{+} satellite cells per isolated muscle fiber from EDL muscles from control tamoxifen-treated *RS6*$^{+/-}$ mice (*n*=51 fibers from 3 mice) compared with tamoxifen-treated *Pax7*$^{CreERT2/+}$;*RS6*$^{+/-}$ mice (*n*=73 fibers from 4 mice). Boxes indicate the interquartile range (IQR), the horizontal line indicates the median, whiskers indicate [1.5 × IQR] and dots indicate the outliers. (F) The dot plot (median indicated by the horizontal line) depicts the number of Pax7^{+} satellite cells per 100 muscle fibers from TA muscles from control tamoxifen-treated *RS6*$^{+/-}$ mice (*n*=6, black dots) compared with tamoxifen-treated *Pax7*$^{CreERT2/+}$;*RS6*$^{+/-}$ mice (*n*=8, white dots).

stands in contrast to previous findings obtained from satellite cell cultures (Ono et al., 2011). We can only speculate about the reasons underlying such discrepancy. Possibly, the effect of Nog as well as of SMAD6 on the BMP target gene *Id1* in our study was too small to alter MyoD transcriptional activity and myogenic lineage progression. Of note, our study lacks experimental proof of whether BMP signaling worked via Id1 to impinge on *MyoD* (*Myod1*) or on other targets. Moreover, previous work demonstrated unchanged satellite cell number in uninjured muscles following *Id* knockout (Clever et al., 2010). Thus, our finding that BMP signaling alters *Id1* expression was useful to demonstrate that BMP signaling was active in cells; however, it offered no explanation of the downstream molecular mechanism. Recent work demonstrated that myogenic proliferation and differentiation can be decoupled (Zalc et al., 2014). In agreement, we found here, following Smad6-induced abrogation of BMP signaling, increased expression of cell cycle inhibitors, notably of *p57* (*Cdkn1c*), which is known to increase stem cell quiescence in conjunction with a decreased proliferation rate (Matsumoto et al., 2011); however, myogenic progression towards myogenin and MHC expression was not altered. This offers a molecular mechanism for the function of BMPs on muscle stem cells, which remains to be explored in detail.

Interestingly, BMP signaling could modulate other signaling cascades, as recently demonstrated for Notch signaling, which becomes activated by BMP-induced Smad1/5 binding to the promoter of the Notch target gene *HES1* in colorectal cancer cells (Irshad et al., 2017). Such BMP-Notch signaling crosstalk, being independent of Id1, could contribute to our observed phenotypes as Notch signaling is a crucial regulator of satellite cell function (Fukada et al., 2011). The dependence of satellite cells on additional signaling systems could well explain why our loss-of-function strategies did not completely abolish satellite cell activity and myofiber growth.

We show that cell-autonomous abrogation of BMP signaling targeted to satellite cells slowed but did not stop accretion of myonuclei. Resulting myofibers, therefore, consist of a mosaic of non-recombined and recombined myonuclei, once recombined satellite cells fuse into the syncytium. This, on the one hand, could signal back on the satellite cells. On the other hand, it could itself retard myofiber growth. Importantly, targeted overexpression of SMAD6 to differentiated muscle (*HSA-Cre*$^{+}$;*RS6*$^{+/-}$ mice) did not affect the number of myonuclei and satellite cells per fiber, thereby providing clear evidence for a direct effect of BMP signaling in satellite cells *in vivo*. Moreover, the myonuclear domain remained unchanged in muscle fibers from *Pax7*$^{CreERT2/+}$;*RS6*$^{+/-}$ mice, suggesting that the cytoplasmic volume per nucleus increased normally during the postnatal growth phase (White et al., 2010). This result stands in contrast to our previous work, which showed, in adult muscle, that decreased BMP signaling causes myofiber atrophy (Sartori et al., 2013).

Whereas we here show smaller satellite cell numbers in *Pax7*$^{CreERT2/+}$;*Alk3*$^{flox/flox}$ mice, the number remained unchanged in *Myf5*^{Cre};*Alk3*$^{flox/flox}$ mice (Huang et al., 2014). This implies that other BMP receptors or signaling pathways other than BMP may

Development (2017) 144, 2737-2747 doi:10.1242/dev.144089

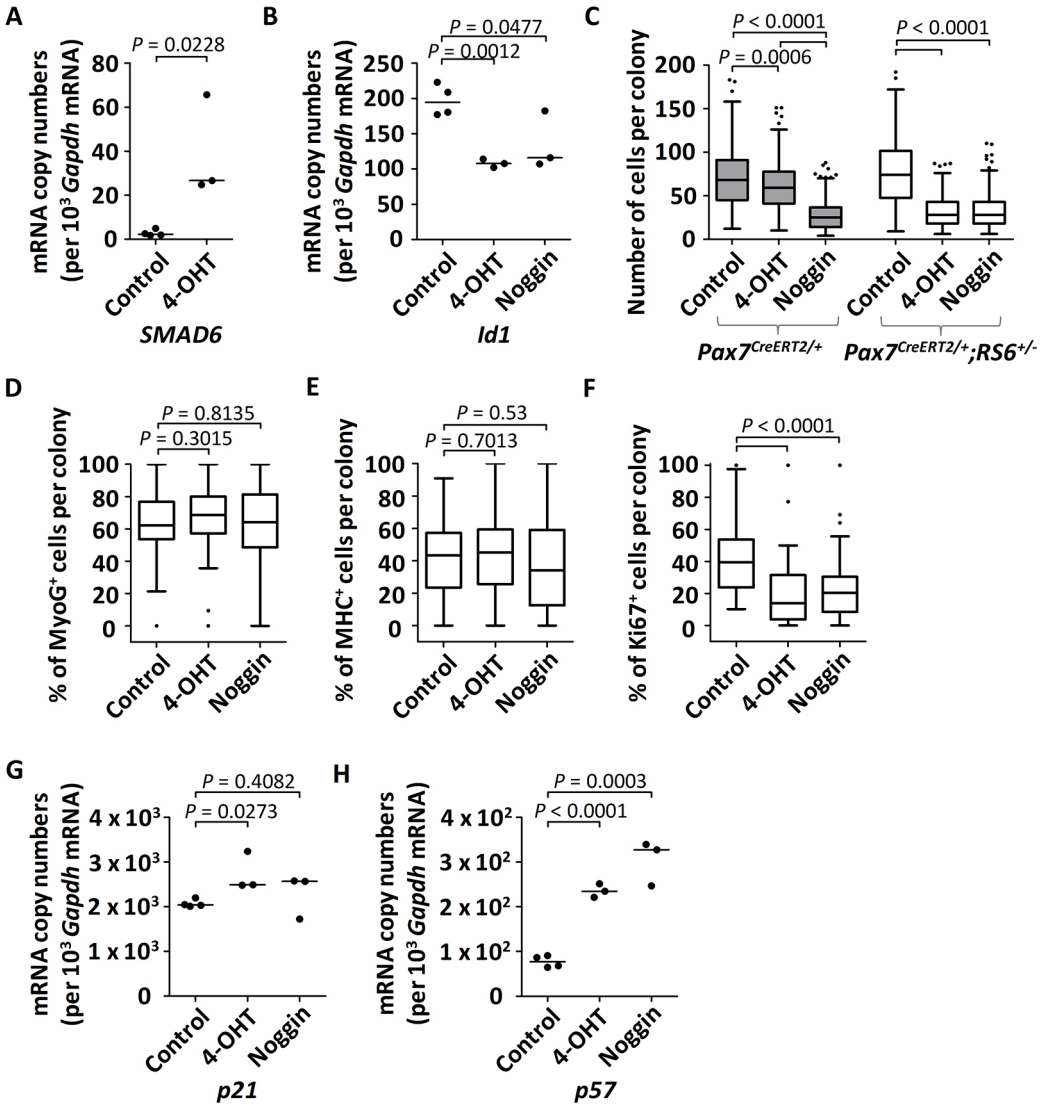

Fig. 7. Quantitative analysis following abrogation of BMP signaling in cultured *Pax7*$^{CreERT2/+}$;*RS6*$^{+/-}$ satellite cell-derived primary myoblasts. Experimental protocol: at day 0, satellite cells from *Pax7*$^{CreERT2/+}$ or *Pax7*$^{CreERT2/+}$;*RS6*$^{+/-}$ adult mice were isolated using FACS and cultured in proliferation media; from days 2-4, cells remained either untreated (control), or were treated with 1 µM hydroxytamoxifen (4-OHT) or with 50 ng/ml of recombinant mouse Nog protein; at day 5, cells were either fixed for immunocytochemistry or collected for RNA extraction. (A,B) The dot plots (median indicated by the horizontal line) depict the relative mRNA copy numbers per 10^3 *Gapdh* mRNA of human *SMAD6* (A) or of the BMP target gene *Id1* (B) from cultured satellite cells isolated from *Pax7*$^{CreERT2/+}$;*RS6*$^{+/-}$ mice. (C) Cells were cultured at low density for a proliferation assay for the comparison of non-treated versus treated satellite cells isolated by FACS from skeletal muscles of *Pax7*$^{CreERT2/+}$ and *Pax7*$^{CreERT2/+}$;*RS6*$^{+/-}$ mice. The number of cells per colony was counted from at least three wells per condition and per mouse (three mice); at least 50 colonies of cells per condition and per mouse were quantified. Data are shown as Whiskers-Tukey box plots. All *P* values were calculated using a *t*-test. (D-F) Following cultures of satellite cells from *Pax7*$^{CreERT2/+}$;*RS6*$^{+/-}$ mice, the number of positive cells is given as a percentage of the total number of stained cells per colony following immunostaining against (D) myogenin (MyoG), (E) myosin heavy chain (MHC) and (F) Ki67. The quantification was performed on 13 to 20 colonies per culture (n=3 cultures, each derived from cells isolated from one mouse, total of n=3 mice). Data are shown as Whiskers-Tukey box plots. All *P* values were calculated using a *t*-test. In C-F, boxes indicate the interquartile range (IQR), the horizontal line indicates the median, whiskers indicate [1.5 × IQR] and dots indicate the outliers. (G,H) Dot plots (median indicated by the horizontal line) depict the relative mRNA copy numbers per 10^3 *Gapdh* mRNA of (G) *p21* and (H) *p57* from FACS-isolated and cultured satellite cells from *Pax7*$^{CreERT2/+}$;*RS6*$^{+/-}$ mice. Cells remained either untreated (control, n=4) or were treated with 1 µM 4-OHT (n=3) or 50 ng/ml of recombinant mouse Nog protein (n=3).

compensate for the deficit in Alk3 in satellite cells. This would be in line with our findings, as Alk3 loss of function in *Pax7*$^{CreERT2/+}$;*Alk3*$^{flox/flox}$ mice resulted in a rather modest effect.

It is now common knowledge that adult muscle satellite cells are of somite origin (Relaix and Marcelle, 2009), but how the expansion of the satellite cell pool is controlled and which factors determine the final number of quiescent satellite cells in the adult stage was unknown. Here, we show that BMP signaling controls the generation of adult satellite cells during the postnatal growth phase. We suggest that BMPs maintain precursor proliferation to generate a sufficiently large precursor cell pool, and cells become quiescent once BMP signaling is withdrawn during muscle maturation.

The exact source and identity of BMPs that control postnatal satellite cell activity remain unknown. Here, we show the presence of BMP transcripts in satellite cells at different time points of postnatal development. However, the respective roles of the various BMPs synthesized by satellite cells and from other sources remain to be determined.

Development (2017) 144, 2737-2747 doi:10.1242/dev.144089

Abnormally high levels of BMP signaling in skeletal muscle can trigger ectopic bone formation, as seen in individuals suffering from fibrodysplasia ossificans progressiva (Shore et al., 2006). Interestingly, myogenic precursors contribute only minimally to BMP-mediated heterotopic ossification (<5%) *in vivo* (Lounev et al., 2009). Using AAV-mediated overexpression of *Bmp4*, we observed an important ossification of soft tissue in the hindlimbs of adult mice after 4 weeks of treatment (data not shown), which is similar to the effects previously reported in the literature (Lounev et al., 2009). Ectopic overexpression of BMP4 likely caused uncontrolled high ligand levels that initiated the osteogenic program in skeletal muscle.

Our results suggest that source, type of BMP ligands, presence of antagonists and expression of receptors must be tightly coordinated to allow correct muscle growth and homeostasis. It remains to be determined whether and how satellite cell-derived BMPs signal to neighboring cells and whether this defines the respective position of satellite cells within their niche. Future BMP gain-of-function experiments and ligand-specific knockout are required to elucidate the role of specific ligands. In conclusion, BMP signaling is an important regulatory pathway during postnatal muscle growth and determines satellite cell-dependent myofiber growth and the size of the adult muscle satellite cell pool.

MATERIALS AND METHODS

Animals

Rosa26-LoxP-Stop-LoxP-huSMAD6-IRES-EGFP transgenic mice (on a *C57BL/6J* background), also labeled *RS6*, were crossbred with the different Cre-driver mice described below. The generation of this mouse line is described in the supplementary Materials and Methods. $Pax7^{CreERT2/+}$ knock-in mice [JAX strain name is *B6;129-Pax7tm2.1(cre/ERT2)Fan/J*] were crossbred with wild-type *C57BL/6J* mice. This strain expresses CRE-ERT2 recombinase from the endogenous *Pax7* locus (Lepper et al., 2009). By crossing $Pax7^{CreERT2/+}$ with the *RS6* strain, we obtained $Pax7^{CreERT2/+}$; $RS6^{+/-}$ offspring. Transgenic *HSA-Cre* mice [JAX strain name *FVB.Cg-Tg (ACTA1-cre)79Jme/J* on a *C57BL/6J* background] have the *Cre* recombinase gene driven by the human α-skeletal actin (*HSA*) promoter (Miniou et al., 1999). By crossing these mice with the *RS6* strain, we obtained *HSA-*$Cre^{+/-}$; $RS6^{+/-}$ offspring. $Alk3^{flox/flox}$ mice (JAX strain name is $Bmpr1a^{tm2.1Bhr}$) contain LoxP sites flanking exon 2 of *Alk3* (Mishina et al., 2002). By crossing $Alk3^{flox/flox}$ with $Pax7^{CreERT2/+}$;$Alk3^{flox/+}$, we obtained $Pax7^{CreERT2/+}$;$Alk3^{flox/flox}$ offspring. The mice were bred in the animal facility of either the Medical Faculty of Paris VI or the Imagine Institute and were kept according to institutional guidelines. Wild-type *C57BL/6J* mice were purchased from Janvier or Charles River. Animal studies have been approved and were carried out under the laboratory and animal facility licenses.

AAV-injection

AAV quantity for intramuscular delivery was calculated relative to total body weight [x(in µl)=1.5×body weight (in g)], which was between 5 and 30 µl. AAV was injected into the triceps brachii muscle or into the muscles of the anterior compartment of the lower leg of 3-day-old *C57BL/6J* mice. Control muscles were either non-injected or injected with PBS as stated in the text and legends. As in previous work, we never observed any effect on muscle morphology or histology in control injected animals when injecting PBS intramuscularly with the exception of some regenerating fibers along the injection trajectory (Sartori et al., 2013). AAV-*Nog* was used at a concentration of 1×10E13 viral genomes (vg)/ml. The plasmid construction and AAV production procedures are described in the supplementary Materials and Methods. At 4 weeks of age, muscles were isolated and prepared for cryosections/histology, qPCR or isolation of single muscle fibers.

Tamoxifen injection for induction of Cre-ERT2 activity

Tamoxifen (Sigma) was prepared in heated corn oil (Sigma) at 37°C at 20 mg/ml and 2.5 µl/g were administered by intra-peritoneal injection into pups (P7 and P9), which were sacrificed at the ages of 1 or 2 months. Adult mice (for primary myoblast cultures, see below), between 2 and 4 months of age, were injected with 100 µl daily for 5 days, and were sacrificed 1 week after the first injection.

FACS isolation and culture of satellite cells

For fluorescent-activated cell sorting, muscles (forelimb, hindlimb, abdominal, pectoral) were processed from P3, P14, P21 and P28 mice. The dissection of the muscles was performed with care to take off as much fat and connective tissue as possible. The muscles were minced in Hank's Balanced Salt Solution (HBSS) supplemented with 0.2% bovine serum albumin, 1% penicillin-streptomycin in a sterile 6 cm Petri dish on ice. The minced muscles were digested for 1.5 h at 37°C with 2 µg/ml collagenase A (Roche), 2.4 U/ml dispase I (Roche), 10 ng/ml DNase I (Roche), 0.4 mM $CaCl_2$ and 5 mM $MgCl_2$ in supplemented HBSS. Cells were washed with supplemented HBSS, filtered through a 100 µm cell strainer and pelleted. The washing step was repeated with 70 µm and finally 40 µm cell strainers.

For labeling extracellular markers, the following primary antibodies were used (10 ng/ml): rat anti-mouse CD45-PE-Cy7 (BD), rat anti-mouse Ter119-PE-Cy7 (BD), rat anti-mouse CD34-BV421 (BD), rat anti-mouse integrin-α7-A700 (R&D Systems) and rat anti-mouse Sca1-FITC (BD). Cells were washed once with ice-cold supplemented HBSS, filtered and re-suspended in supplemented HBSS. Flow cytometric analysis and cell sorting were performed on a FACSAriaII (BD) previously calibrated (Fluorescence Minus One and use of compensation beads) using the Lumic-CyPS UPMC platform. TER119 $(LY76)^+$ and CD45 (PTPRC, $LY5)^+$ cells were negatively selected, $CD34^+$ and integrin-$\alpha7^+$ cells were positively selected and the remaining cells were gated based on $SCA1^-$ expression. The selected cells were collected in a FACS tube containing lysis buffer and were directly processed for RNA extraction as described below.

Culture of satellite cell-derived primary myoblasts using the pre-plating method

Cells from adult muscle tissue, prepared in a similar way to the method used for the FACS purification procedure, were resuspended in growth medium (see FACS procedure) and pre-plated onto a non-coated 15 cm Petri dish for 4 h (fibroblasts will adhere to the plate, whereas most myoblasts will remain in suspension). The media contained myoblasts in suspension and was transferred onto gelatin-coated 10 cm Petri dishes. Cultures were maintained in growth medium until cells reached 70% confluency, after which cells were harvested by trypsinization for RNA extraction.

MACS isolation and culture of satellite cells

Satellite cells were isolated from forelimb, hindlimb and back muscles of 6- to 8-week-old female C57BL/6 mice using the skeletal muscle dissociation kit (Miltenyi Biotech, 130-098-305) followed by magnetic-activated cell sorting (MACS). MACS separation involved an initial enrichment step using the mouse satellite cell isolation kit (Miltenyi Biotech, 130-104-268) followed by further purification with mouse anti-integrin α-7 microbeads (Miltenyi Biotech, 130-104-261). Isolated cells were plated on growth factor reduced matrigel (Corning)-coated dishes in medium containing DMEM (Gibco), 15% FBS (Gibco), 2.5 ng/ml basic FGF (Sigma), 10 ng/ml leukemia inhibitory factor (BioChrom) and 1% Pen/Strep (Gibco), and maintained in a humidified hypoxic 3% O_2/5% CO_2 atmosphere at 37°C. After the first 24 h in culture, 1× B27 without vitamin A (Gibco) was added to the medium. Following a 2-day culture period, which permitted sufficient expansion of the satellite cells without loss of Pax7 positivity, cells were treated with 100 ng/ml recombinant human BMP4 (R&D Systems, 314-BP) or with the vehicle used to reconstitute BMP4 (4 mM HCl containing 0.1% bovine serum albumin) in a serum-free medium. Prior to incubation with BMP4, cells were switched to a serum-free medium for 6 h to eliminate the effect from unknown BMP signaling components in the serum. Where specified, BMP soluble receptor (recombinant mouse BMPR-IA/ALK3-Fc Chimera, R&D Systems, 437-MR) in a concentration of 200 ng/ml was added to the medium to block residual BMP signaling components. Following cell harvest, cells were immediately lysed and total RNA was extracted using the RNeasy Micro kit (Qiagen). Reverse transcription was performed using SuperScript III Reverse Transcriptase (Invitrogen).

Development (2017) 144, 2737-2747 doi:10.1242/dev.144089

Quantitative real-time PCR (RT-qPCR) was performed on the 7000 Sequence Detection System (Applied Biosystems) using SYBR Green I detection chemistry (Applied Biosystems).

RNA isolation and real-time PCR

Total RNA from frozen muscle tissue was isolated using Trizol (Invitrogen) extraction in combination with RNeasy Mini kit (Qiagen). Total RNA from FACS-isolated satellite cells was isolated using the RNAqueous Microkit (Ambion kit, Life Technologies). Total RNA from cultured primary myoblasts was isolated using the RNeasy Micro kit (Qiagen). In all cases, RNase-Free DNase I Set (Qiagen or Life Technologies) was used to eliminate traces of DNA in the RNA extract. Isolated RNA was quantified using NanoVue Plus GE HealthCare spectrophotometer (Dutscher). For RNA extracted from muscle tissue and from cultured myoblasts, cDNA synthesis was performed using the ThermoScript RT-PCR system (Invitrogen) with random hexamer primers for first-strand cDNA synthesis. For RNA extracted from FACS-isolated satellite cells, cDNA synthesis was performed using SuperScript VILO Master Mix (Invitrogen). Real-time polymerase chain reaction (RT-qPCR) was performed according the SYBR Green protocol (BioRad) in triplicate on the CFX96 Touch Real-Time detection system (BioRad) using iTaq Universal SYBR Green Supermix (BioRad). Alternatively, reverse transcription was performed using SuperScript III Reverse Transcriptase (Invitrogen), followed by RT-qPCR on the 7000 Sequence Detection System (Applied Biosystems) using SYBR Green I detection chemistry (Applied Biosystems). A 10 min denaturation step at 94°C was followed by 40 cycles of denaturation at 94°C for 10 s and annealing/extension at 60°C for 30 s. Before sample analysis, we had determined for each gene and primer set the PCR efficiencies with a standard dilution series (10E1-10E7 copies/µl), which subsequently enabled us to determine the copy numbers from the C_t values. mRNA levels were normalized to 10E3 or 10E6 copies of *Gapdh* mRNA. Fold changes were calculated according to the efficiency corrected $-\Delta\Delta C_t$ method (Pfaffl, 2001). The sequences for the primers used are listed in Table S1.

Immunocytochemistry/immunohistochemistry

Immunocytochemistry/histological analyses were performed using primary antibodies against Pax7 (1/50 mouse IgG1 from DSHB or alternatively 1/2 mouse IgG1 DSHB-hybridoma cell supernatant), pSmad1/5 (1/50, rabbit, Cell Signaling, 9516), laminin (1/400, rabbit, Dako, Z0097), anti-BrdU (1/100, rat, Abcam, ab6326), m-Cadherin (1/50, mouse IgG1, Nanotools, 0106-100), MyoD (1/100, rabbit IgG1, Santa Cruz Biotechnology, sc760), myogenin (1/100, mouse IgG1, DSHB), panMHC (mouse Ig2a, A4-1025, DSHB), Ki67 (1/100, mouse IgG1, BD Biosciences, 556003) and cleaved-caspase 3 (1/300, Cell Signaling, 9664), followed by secondary antibodies with various fluorophores (Alexa Fluor 1/400 goat anti-mouse IgG1 488 or 594, goat anti-rabbit 488 or 594) and DAPI (1/1000 or 1/5000, Sigma). Fluorescence was visualized using a Zeiss Axio Imager with an Orkan camera (Hamamatsu) and AxioVision software.

Fluorescence intensity quantification

All parameters during image acquisition were kept the same. Fluorescence intensity was quantified using ImageJ software. The background was removed and the regions of interest (ROIs; in this case nuclei) were identified using the software 'Nucleus Counter' plug-in. 'Integrated Density' and 'Area' measurements were performed for each nucleus and the corrected fluorescence intensity was calculated as follows: corrected fluorescence intensity=integrated density÷area.

BrdU analysis

Mice were treated with AAV-*Nog* or AAV-control, which were intramuscularly injected into the tibialis anterior (TA) muscle at P3. At P14, animals were labeled with BrdU (Invitrogen) by subcutaneous injection with 10 µl per 1 g body weight for 3 consecutive days. Following sacrifice, histological sections of the TA muscle (12 µm) were fixed with 4% paraformaldehyde for 10 min and permeabilized with methanol (−20°C) for 6 min. Antigens were retrieved by boiling for 30 min at 70-80°C in 0.01 M sodium nitrate (pH 6). This was followed by incubation with HCl (1 N) for 20 min at 37°C. Samples were washed in PBS and incubated for 1 h in blocking buffer (2% BSA and 2% porcine serum). Samples were incubated overnight at 4°C with anti-BrdU (rat, Abcam) in combination with other primary antibodies (see above).

Western blot

Proteins were extracted from frozen triceps brachii muscle using RIPA buffer with a proteinase and phosphatase inhibitor cocktail (Complete tablets, Roche). Proteins were separated through denaturating SDS-polyacrylamide gel electrophoresis with the Laemmli system and transferred onto nitrocellulose membranes using the wet method (BioRad). The blots were probed using primary antibodies against GFP (1/5000, Aves Labs) and Actin (1/10000, Sigma). Western blots were analyzed with SuperSignal West Pico Chemiluminescent substrate (Pierce).

Single fiber preparation

Mice were sacrificed at P3 and P28. TA and extensor digitorum longus (EDL) muscles were surgically isolated. Muscles were thereafter digested in 0.2% collagenase type 1 dissolved in DMEM (Life Technologies). Individual, viable, undamaged myofibers were isolated by gently passing them through Pasteur pipettes with different sized apertures as described in detail elsewhere (Moyle and Zammit, 2014). Then the myofibers were fixed in 4% paraformaldehyde dissolved in PBS (Sigma) for 10 min, washed, stained against Pax7 (1/50, mouse IgG1, DSHB) and with DAPI, and mounted on slides.

Morphometric studies

Cryosections of 12 µm of TA muscles were stained with anti-laminin to delineate the muscle fibers and anti-Pax7 or anti-m-Cadherin to label satellite cells. Fluorescent photographs were taken with a ×20 objective on a microscope (Zeiss, AxioImage) and saved as TIFF files. These images were projected onto a flatscreen coupled with a graphic tablet, which enabled the manual retracing of the muscle fiber outlines and the counting of satellite cells. The fibers of the entire muscle cross-section were analyzed.

For myonuclear domain analysis, single fibers were stained with Pax7 and DAPI. Images of at least three different segments of each fiber were acquired with a ×40 objective on a microscope (Zeiss, AxioImage) and the number of $Pax7^-$ nuclei was quantified. The volume of each fiber segment was then assessed on the acquired images by measuring with ImageJ software the length (L) of the fiber segment and the fiber diameter (D) as follows: $volume=\pi\times(D\div2)^2\times L$. The myonuclear domain was then calculated as follows: myonuclear domain=volume÷number of nuclei.

Statistical analysis

The results are expressed as the mean together with the standard error of the mean (s.e.m.) for qPCR data. Other data are presented as dot plots of the median or as Whiskers-Tukey box plots. The probability for statistical differences between two experimental groups was determined through calculation of the *P* value using the two-tailed unpaired *t*-test.

Acknowledgements

We thank Dr Yuji Mishina (University of Michigan, Ann Arbor, MI, USA) for providing the *Alk3*$^{fl/fl}$ mice.

Competing interests

The authors declare no competing or financial interests.

Author contributions

Conceptualization: F.L.G., L.G., C. Birchmeier, T.B., M.S., F.R., H.A.; Methodology: S.S., S.A.-M., T.B.; Validation: A.S., E.S., S.S., T.B., M.S., F.R., H.A.; Formal analysis: A.S., E.S., I.P., F.Z.; Investigation: A.S., E.S., S.A.-M., I.P., F.Z., E.M.; Resources: S.S., C. Beley, A.J., C.C., T.B.; Writing - original draft: A.S., E.S., M.S., H.A.; Writing - review & editing: A.S., E.S., S.S., S.A.-M., I.P., E.M., F.L.G., C. Birchmeier, T.B., M.S., H.A.; Visualization: A.S., E.S., M.S., H.A.; Supervision: C. Birchmeier, T.B., M.S., F.R., H.A.; Project administration: C. Birchmeier, T.B., M.S., F.R., H.A.; Funding acquisition: A.S., E.S., C. Birchmeier, T.B., M.S., F.R., H.A.

Funding

This work was supported by the Association Française contre les Myopathies (AFM) to E.M., C. Beley, L.G., F.R. and H.A.; by the Agence Nationale de la Recherche (ANR) to F.R. and H.A. (ANR-12-BSV10038, ANR-16-CE14-0002-01), and to C.C.

and F.R. (ANR-13-BSV1-0011); by the National Institutes of Health-National Institute of Arthritis and Musculoskeletal and Skin Diseases to C.C. (R01 AR057344); by the Deutsche Forschungsgemeinschaft (DFG) to A.S., M.S. and C. Birchmeier (as part of the MyoGrad International Graduate School for Myology, GK 1631/1); by the Fondation pour la Recherche Médicale (FRM) to A.S. (FDT20140930879); by the Ministère de l'Enseignement Supérieur et de la Recherche to E.S. and A.J.; and by the Université Franco-allemande (UFA, as part of the MyoGrad International Graduate School for Myology, CDFA-06-11) to E.S., A.S., I.P., F.R., H.A., C. Birchmeier, L.G. and M.S. The funders had no role in study design, data collection and analysis, decision to publish, or preparation of the manuscript. Deposited in PMC for release after 12 months.

Supplementary information

Supplementary information available online at
http://dev.biologists.org/lookup/doi/10.1242/dev.144089.supplemental

References

Amthor, H., Christ, B., Weil, M. and Patel, K. (1998). The importance of timing differentiation during limb muscle development. *Curr. Biol.* **8**, 642-652.

Amthor, H., Christ, B. and Patel, K. (1999). A molecular mechanism enabling continuous embryonic muscle growth - a balance between proliferation and differentiation. *Development* **126**, 1041-1053.

Amthor, H., Christ, B., Rashid-Doubell, F., Kemp, C. F., Lang, E. and Patel, K. (2002). Follistatin regulates bone morphogenetic protein-7 (BMP-7) activity to stimulate embryonic muscle growth. *Dev. Biol.* **243**, 115-127.

Beilharz, M. W., Lareu, R. R., Garrett, K. L., Grounds, M. D. and Fletcher, S. (1992). Quantitation of muscle precursor cell activity in skeletal muscle by Northern analysis of MyoD and myogenin expression: application to dystrophic (mdx) mouse muscle. *Mol. Cell. Neurosci.* **3**, 326-331.

Clever, J. L., Sakai, Y., Wang, R. A. and Schneider, D. B. (2010). Inefficient skeletal muscle repair in inhibitor of differentiation knockout mice suggests a crucial role for BMP signaling during adult muscle regeneration. *Am. J. Physiol. Cell Physiol.* **298**, C1087-C1099.

Fukada, S.-i., Yamaguchi, M., Kokubo, H., Ogawa, R., Uezumi, A., Yoneda, T., Matev, M. M., Motohashi, N., Ito, T., Zolkiewska, A. et al. (2011). Hesr1 and Hesr3 are essential to generate undifferentiated quiescent satellite cells and to maintain satellite cell numbers. *Development* **138**, 4609-4619.

Goto, K., Kamiya, Y., Imamura, T., Miyazono, K. and Miyazawa, K. (2007). Selective inhibitory effects of Smad6 on bone morphogenetic protein type I receptors. *J. Biol. Chem.* **282**, 20603-20611.

Hirsinger, E., Duprez, D., Jouve, C., Malapert, P., Cooke, J. and Pourquie, O. (1997). Noggin acts downstream of Wnt and Sonic Hedgehog to antagonize BMP4 in avian somite patterning. *Development* **124**, 4605-4614.

Huang, P., Schulz, T. J., Beauvais, A., Tseng, Y.-H. and Gussoni, E. (2014). Intramuscular adipogenesis is inhibited by myo-endothelial progenitors with functioning Bmpr1a signalling. *Nat. Commun.* **5**, 4063.

Irshad, S., Bansal, M., Guarnieri, P., Davis, H., Al Haj Zen, A., Baran, B., Pinna, C. M. A., Rahman, H., Biswas, S., Bardella, C. et al. (2017). Bone morphogenetic protein and Notch signalling crosstalk in poor-prognosis, mesenchymal-subtype colorectal cancer. *J. Pathol.* **242**, 178-192.

Jen, Y., Weintraub, H. and Benezra, R. (1992). Overexpression of Id protein inhibits the muscle differentiation program: in vivo association of Id with E2A proteins. *Genes Dev.* **6**, 1466-1479.

Krause, C., Guzman, A. and Knaus, P. (2011). Noggin. *Int. J. Biochem. Cell Biol.* **43**, 478-481.

Lepper, C., Conway, S. J. and Fan, C.-M. (2009). Adult satellite cells and embryonic muscle progenitors have distinct genetic requirements. *Nature* **460**, 627-631.

Lounev, V. Y., Ramachandran, R., Wosczyna, M. N., Yamamoto, M., Maidment, A. D. A., Shore, E. M., Glaser, D. L., Goldhamer, D. J. and Kaplan, F. S. (2009). Identification of progenitor cells that contribute to heterotopic skeletogenesis. *J. Bone Joint Surg.* **91**, 652-663.

Matsumoto, A., Takeishi, S., Kanie, T., Susaki, E., Onoyama, I., Tateishi, Y., Nakayama, K. and Nakayama, K. I. (2011). p57 is required for quiescence and maintenance of adult hematopoietic stem cells. *Cell Stem Cell* **9**, 262-271.

Mauro, A. (1961). Satellite cell of skeletal muscle fibers. *J. Biophys. Biochem. Cytol.* **9**, 493-495.

Miniou, P., Tiziano, D., Frugier, T., Roblot, N., Meur, M. L. and Melki, J. (1999). Gene targeting restricted to mouse striated muscle lineage. *Nucl. Acids Res.* **27**, e27-e30.

Mishina, Y., Hanks, M. C., Miura, S., Tallquist, M. D. and Behringer, R. R. (2002). Generation of Bmpr/Alk3 conditional knockout mice. *Genesis* **32**, 69-72.

Miyazono, K. and Miyazawa, K. (2002). Id: a target of BMP signaling. *Sci. STKE* **2002**, pe40.

Moyle, L. A. and Zammit, P. S. (2014). Isolation, culture and immunostaining of skeletal muscle fibres to study myogenic progression in satellite cells. *Methods Mol. Biol.* **1210**, 63-78.

Nohe, A., Hassel, S., Ehrlich, M., Neubauer, F., Sebald, W., Henis, Y. I. and Knaus, P. (2002). The mode of bone morphogenetic protein (BMP) receptor oligomerization determines different BMP-2 signaling pathways. *J. Biol. Chem.* **277**, 5330-5338.

Nohe, A., Keating, E., Knaus, P. and Petersen, N. O. (2004). Signal transduction of bone morphogenetic protein receptors. *Cell. Signal.* **16**, 291-299.

Ono, Y., Calhabeu, F., Morgan, J. E., Katagiri, T., Amthor, H. and Zammit, P. S. (2011). BMP signalling permits population expansion by preventing premature myogenic differentiation in muscle satellite cells. *Cell Death Differ.* **18**, 222-234.

Pfaffl, M. W. (2001). A new mathematical model for relative quantification in real-time RT–PCR. *Nucl. Acids Res.* **29**, e45.

Pourquié, O., Fan, C.-M., Coltey, M., Hirsinger, E., Watanabe, Y., Bréant, C., Francis-West, P., Brickell, P., Tessier-Lavigne, M. and Le Douarin, N. M., (1996). Lateral and axial signals involved in avian somite patterning: a role for BMP4. *Cell* **84**, 461-471.

Relaix, F. and Marcelle, C. (2009). Muscle stem cells. *Curr. Opin. Cell Biol.* **21**, 748-753.

Sartori, R., Schirwis, E., Blaauw, B., Bortolanza, S., Zhao, J., Enzo, E., Stantzou, A., Mouisel, E., Toniolo, L., Ferry, A. et al. (2013). BMP signaling controls muscle mass. *Nat. Genet.* **45**, 1309-1318.

Shore, E. M., Xu, M., Feldman, G. J., Fenstermacher, D. A., Cho, T.-J., Choi, I. H., Connor, J. M., Delai, P., Glaser, D. L., LeMerrer, M. et al. (2006). A recurrent mutation in the BMP type I receptor ACVR1 causes inherited and sporadic fibrodysplasia ossificans progressiva. *Nat. Genet.* **38**, 525-527.

Tylzanowski, P., Mebis, L. and Luyten, F. P. (2006). The Noggin null mouse phenotype is strain dependent and haploinsufficiency leads to skeletal defects. *Dev. Dyn.* **235**, 1599-1607.

Wang, H., Noulet, F., Edom-Vovard, F., Le Grand, F. and Duprez, D., (2010). Bmp signaling at the tips of skeletal muscles regulates the number of fetal muscle progenitors and satellite cells during development. *Dev. Cell* **18**, 643-654.

White, R. B., Biérinx, A.-S., Gnocchi, V. F. and Zammit, P. S. (2010). Dynamics of muscle fibre growth during postnatal mouse development. *BMC Dev. Biol.* **10**, 21.

Zalc, A., Hayashi, S., Auradé, F., Bröhl, D., Chang, T., Mademtzoglou, D., Mourikis, P., Yao, Z., Cao, Y., Birchmeier, C. et al. (2014). Antagonistic regulation of p57kip2 by Hes/Hey downstream of Notch signaling and muscle regulatory factors regulates skeletal muscle growth arrest. *Development* **141**, 2780-2790.

SUPPLEMENTARY MATERIALS

Figure S1 – (A) Gene expression dynamics of BMP signaling pathway components in skeletal muscle from neonatal and juvenile mice. Diagrams depict the relative mRNA copy numbers per 10^3 *Gapdh* mRNA copies of different BMP ligands (*Bmp2*, *4*, *5*, *6*, *7*, *13*, *14*), BMP type I receptor *Alk3*, BMP target gene *Id1*, BMP antagonists *Nog* (encoding Noggin), *Grem1* (encoding Gremlin), *Fst* (encoding Follistatin), and *Chrd* (encoding Chordin) in skeletal muscles from wildtype mice (n=3 biological and n=3 technical replicates) at P3 (black), P14 (white), P21 (dark grey) and P28 (light grey). Values are shown as mean ± SEM. **(B-D) Evaluation of BMP responsiveness of satellite cells *in vitro*.** Cultured mouse satellite cells, which were MACS isolated, were incubated for 1 hour with vehicle or with 100 ng/ml BMP4. Prior to BMP4 stimulation cells were switched for 6 h to serum-free medium containing 200 ng/ml soluble Alk3 receptor (sAlk3). This was done to prevent binding of BMP ligands that were likely present in the culture medium. **(B)** Exemplary images of immunostainings of MACS-isolated and cultured satellite cells expressing phosphorylated Smad1/5 (red) and Pax7 (green). DAPI (blue) was used as a nuclear stain. Scale bar 0.5 µm. **(C)** The Whiskers-Tukey box plot depicts the phosphorylated Smad1/5 fluorescent staining intensity per nuclear area in the BMP4 treated as opposed to the Vehicle treated satellite cells. A minimum of 200 nuclei was analyzed for each condition. **(D)** Time course of *Id1* mRNA expression following 0 h, 0.5 h, 1.0 h, 2.0 h, 3.0 h, and 4.0 h of BMP4 stimulation. Cultured mouse satellite cells, which were MACS isolated, were incubated with vehicle (in grey) or with 100 ng/ml BMP4 (in black) over the indicated time periods to assess *Id1* mRNA expression levels. Prior to vehicle or BMP4 treatment, cells were switched to a serum-free medium containing 200 ng/ml sAlk3 for 6 h. Three different controls are depicted: non serum starved cells (control with serum, in stripes), serum starved cells (control w/o serum, in white) and serum starved with sAlk3 (control w/o serum, and with sAlk3, in black dots). Values are depicted as mean ± S.E.M (n=3).

Figure S1

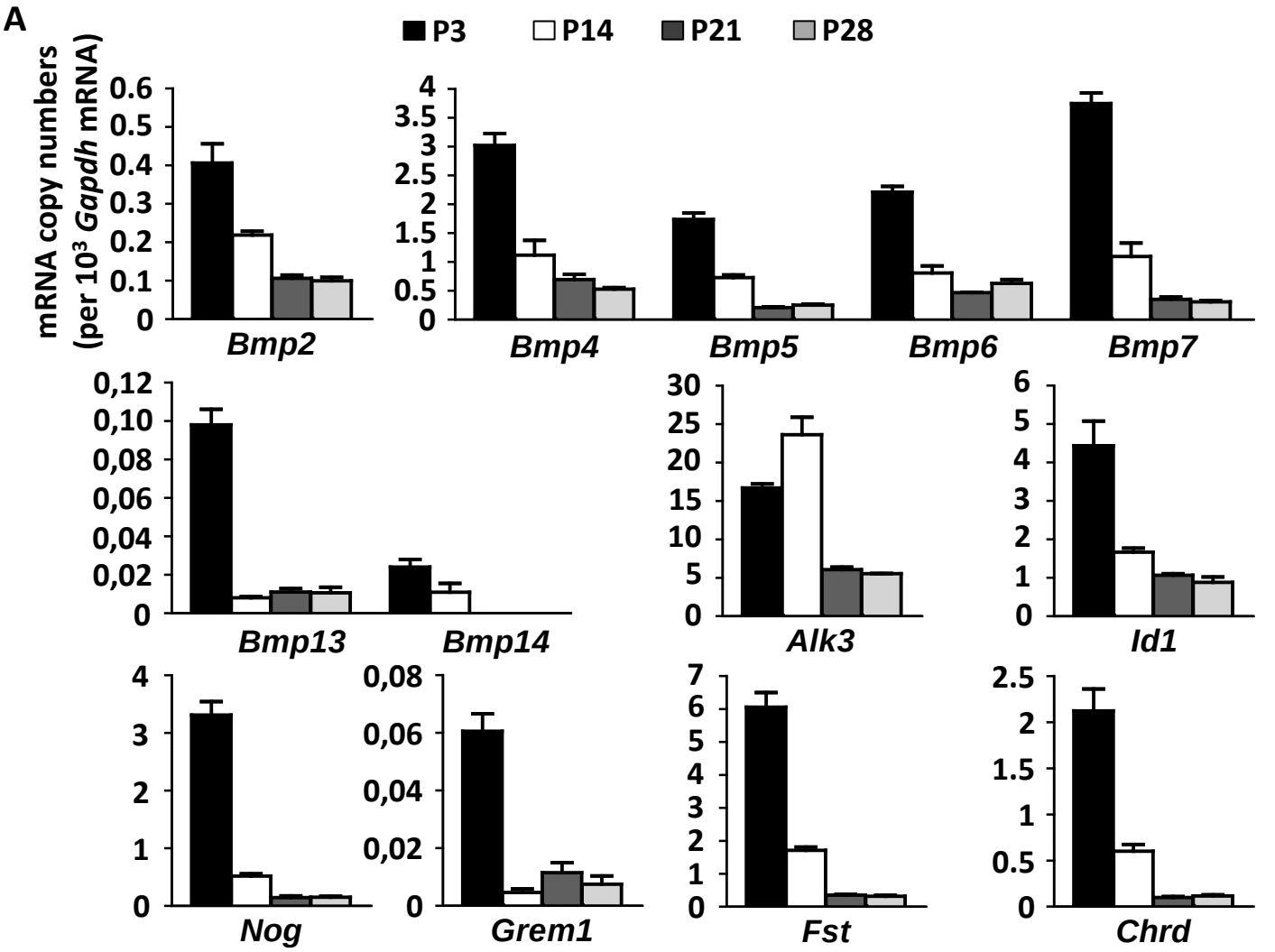

Figure S2 – (A-E) Consequences of Noggin mediated abrogation of BMP signaling for juvenile muscle growth. (A) The diagram presents the gene expression of *Nog* (chicken origin) in muscles from control and AAV-*Nog* injected mice (two weeks following the injection, n=4). Data represent mRNA copies per 10^3 *Gapdh* mRNA copies and are shown as dot plots (+median). **(B)** The histogram presents the distribution of myofiber diameter of single myofibers isolated from *TA* muscles of 4-week-old mice. Dashed lines represent the fitted normal distribution. n=107 and n=128 myofibers were analyzed, respectively, from 3 non-injected control and 5 AAV-*Nog* treated muscles at P3. **(C)** The Whiskers-Tukey box plots depict the myofiber length. n=65 and n=103 myofibers, respectively, from three non-injected control and five AAV-*Nog* treated muscles at P3. **(D)** Exemplary images of isolated single fibers of *TA* muscle from day P3 old mice (left panel) and 4-week-old mice (right panel). The inlays show a magnified section of the fibers. Fibers were stained with DAPI and tiled images were acquired using an automated microscope. Fluorescent images were superimposed over transmission light images. Scale bar 500 µm. **(E)** Exemplary images of immunostaining on a *TA* muscle of 4-week-old mice. The muscle was injected with saline solution (control, left panel) or AAV-*Nog* treated at P3 (right panel). The images illustrate the number of $Pax7^+$ satellite cells (red, arrows) and the size of the myofibers delineated by laminin (green). DAPI (blue) was used as a nuclear stain. Scale bar 20 µm. **(F-J) Consequences of Cre/Lox mediated SMAD6 overexpression in satellite cells. (F)** Mice were injected with tamoxifen for 5 consecutive days and were sacrificed one week after the first tamoxifen injection; skeletal muscles were collected and processed to isolate satellite cell-derived primary myoblasts with the pre-plating method; cells were cultured in proliferation medium for 4 days after which the RNA was extracted. The image depicts a 1.5% agarose gel supplemented with ethidium bromide showing the presence or absence of the *huSMAD6* PCR product (using primers specific for the human sequence). The PCR was performed on cDNA synthesized from RNA extracted from cultured satellite cell-derived primary myoblasts from either tamoxifen treated $Pax7^{CreERT2/+}$ control mice (lane 2) or tamoxifen treated $Pax7^{CreERT2/+}$;$RS6^{+/-}$ mice (lane 3). The presence of the band in lane 3 reflects that recombination occurred under these experimental conditions. Lane 1: 100 bp size marker. **(G-I)** $RS6^{+/-}$ and $Pax7^{CreERT2/+}$;$RS6^{+/-}$ mice were injected with tamoxifen at P7 and P9, and sacrificed at the age of two months. **(G)** Fluorescence images of mid-belly transverse sections of *TA* muscles from control tamoxifen treated $RS6^{+/-}$ mice in comparison to tamoxifen treated $Pax7^{CreERT2/+}$;$RS6^{+/-}$ mice, immunostaining against Pax7 in red (arrows), against Laminin (green), nuclei stained with DAPI (blue). Scale bar 20 µm. **(H)** Whiskers-Tukey box plots depict the quantification of the fibers diameters of *TA* muscle, analyzed on mid-belly muscle sections following immunostaining against Laminin, from control tamoxifen treated $RS6^{+/-}$ mice (n=3, grey) in comparison to tamoxifen treated $Pax7^{CreERT2/+}$;$RS6^{+/-}$ mice (n=3, white). **(I)** Histogram presenting the distribution of *TA* muscle fiber diameters. **(J)** Dot plot (+median) depicts the number of $Pax7^+$ nuclei quantified per 100 myofibers on *TA* mid-belly transverse muscle sections from control tamoxifen treated $RS6^{+/-}$ mice (n=3, black circles) in comparison to tamoxifen treated $Pax7^{CreERT2/+}$;$RS6^{+/-}$ mice (n=3, white circles).

Figure S2

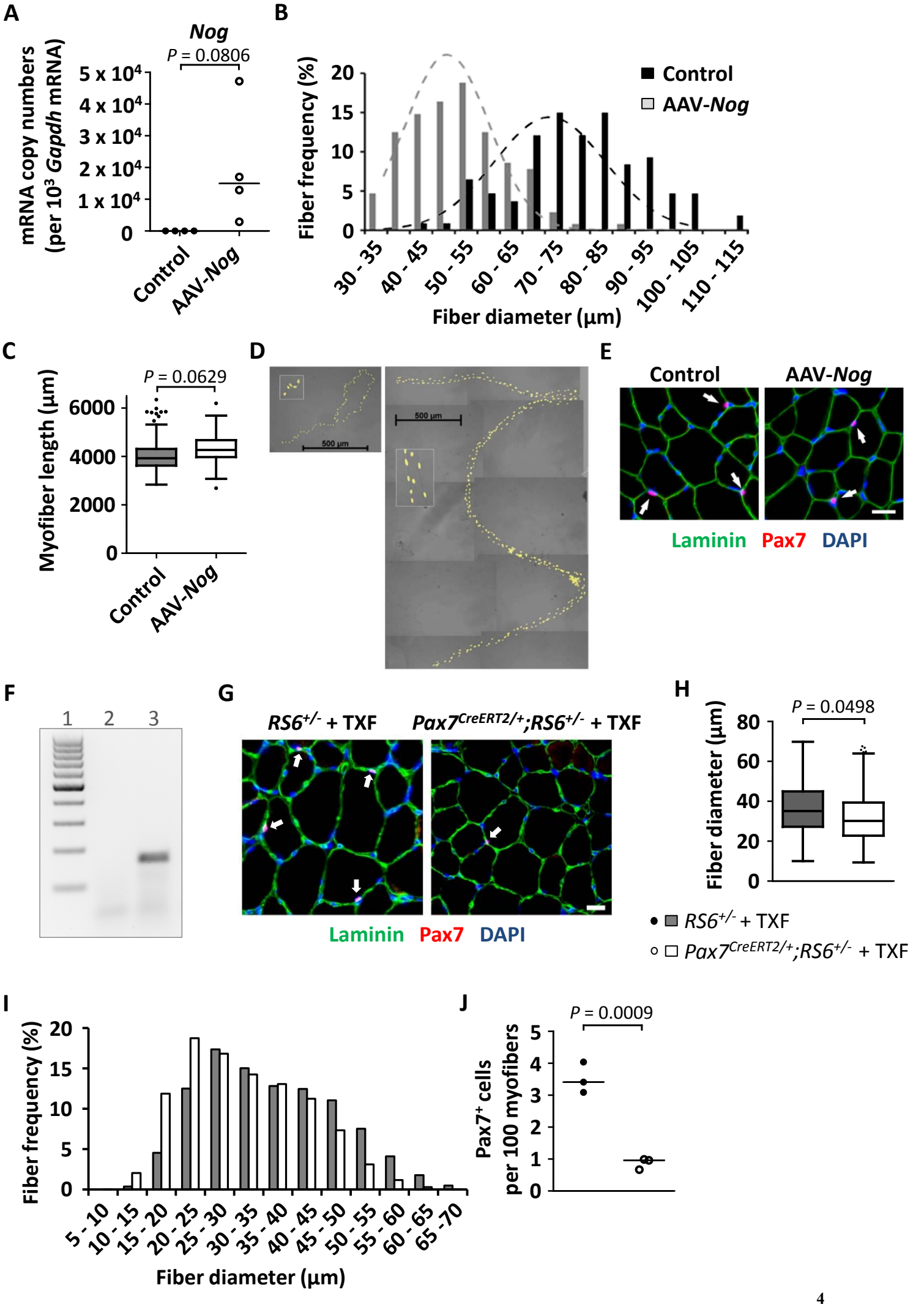

Figure S3 – Effect of SMAD6 overexpression in differentiated muscle. (A) Image of immunoblots showing GFP and actin bands, along with the Ponceau staining as loading control. Total proteins were extracted from the *triceps* muscle of two *HSA-Cre*$^{+}$*;RS6*$^{+/-}$ mice and two *RS6*$^{+/-}$ mice at 1 month of age. **(B)** The dot plots (+median) depict the relative mRNA copy numbers per 10^{6} *GAPDH* mRNA of *huSMAD6*. RNA was extracted from the *gastrocnemius* muscle of 1-month-old *RS6*$^{+/-}$ mice (n=3, black dots) and *HSA-Cre*$^{+}$*;RS6*$^{+/-}$ mice (n=5, white dots). **(C)** Example of hematoxylin and eosin staining (HE, upper panel) on mid-belly transverse sections of the *TA* muscle from 1-month-old control *HSA-Cre*$^{+}$ mice (left panel) in comparison to *HSA-Cre*$^{+}$*;RS6*$^{+/-}$ mice (right panel). Scale bar 40 μm. Example of a fluorescence image (lower panel) following immunostaining against Pax7 (red, arrows), against Laminin (green) and nuclei stained with DAPI (blue) of mid-belly transverse sections of *TA* muscle from 2-month-old control *HSA-Cre*$^{+}$ mice (left panel) in comparison to *HSA-Cre*$^{+}$*;RS6*$^{+/-}$ mice (right panel). Scale bar 20 μm. **(D)** Dot plots (+median) depicting the number of Pax7^{+} satellite cells per 100 myofibers counted on *TA* mid-belly muscle sections from 1-month-old control *RS6*$^{+/-}$ mice (n=3) in comparison to *HSA-Cre*$^{+}$*;RS6*$^{+/-}$ mice (n=5). **(E)** Dot plots (+median) depicting the number of Pax7^{+} satellite cells per 100 myofibers counted on *TA* mid-belly muscle sections from 2-month-old control *RS6*$^{+/-}$ mice (n=4) in comparison to *HSA-Cre*$^{+}$*;RS6*$^{+/-}$ mice (n=4).

Figure S3

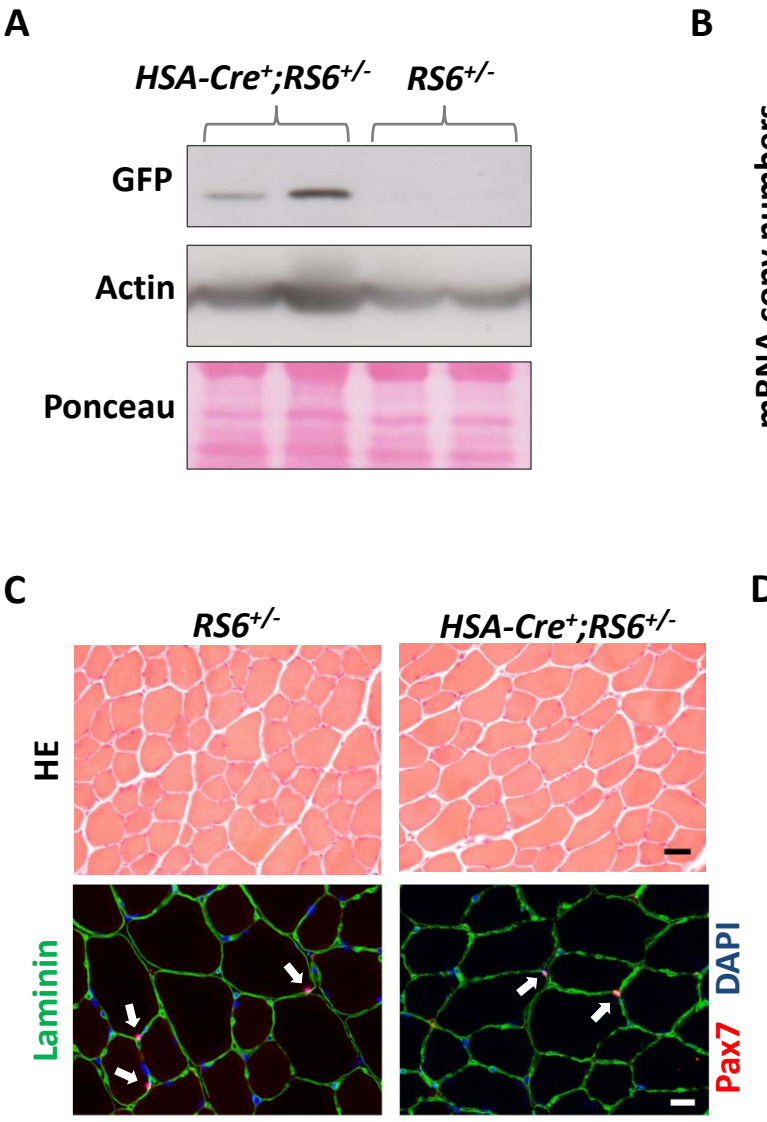

Figure S4 – Analysis of cell proliferation and differentiation following abrogation of BMP signaling in cultured *Pax7*$^{CreERT2/+}$;*RS6*$^{+/-}$ satellite cell-derived primary myoblasts. **(A)** Scheme of the experimental protocol: at day 0 satellite cells from *Pax7*$^{CreERT2/+}$;*RS6*$^{+/-}$ adult mice were isolated using FACS and cultured in low density with proliferation media; from days 2-4 they remained either untreated (control), or were treated with 1 μM hydroxytamoxifen (4-OHT) or 50 ng/mL of recombinant mouse Noggin protein (Noggin); at day 5 cells were fixed for immunocytochemistry. **(B)** Representative fluorescence images of single colonies in which nuclei stained with DAPI are blue and immunostaining against MyoD, myogenin (MyoG), myosin heavy chain (MHC), or Ki67 in red (from top to bottom). Scale bar 100 μm. **(C-E)** Data are shown as cumulative rank ogives of the number of myoblasts, in a colony, expressing the protein of interest marked by immunofluorescence. Different culture conditions are compared (control in blue, treated with 4-OHT in red and treated with Noggin in green). The number of cells that are positively stained for Myogenin (MyoG) **(C)**, Myosin heavy chain **(D)** and Ki67 **(E)** are plotted on the horizontal axis. The vertical axis corresponds to the individual ranks, normalized to the total rank for each experiment to permit comparison of data sets of different sample size. The quantification was performed on 13 to 20 colonies per culture (n=3 cultures, each derived from cells isolated from one mouse, total of n=3 mice).

Figure S4

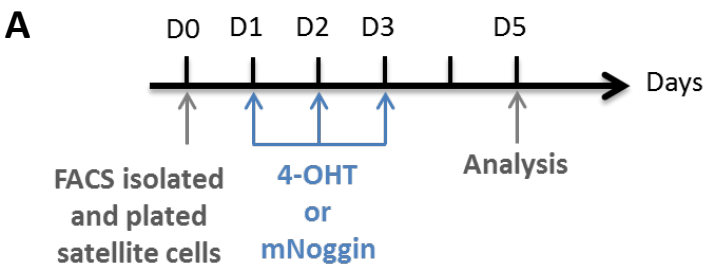

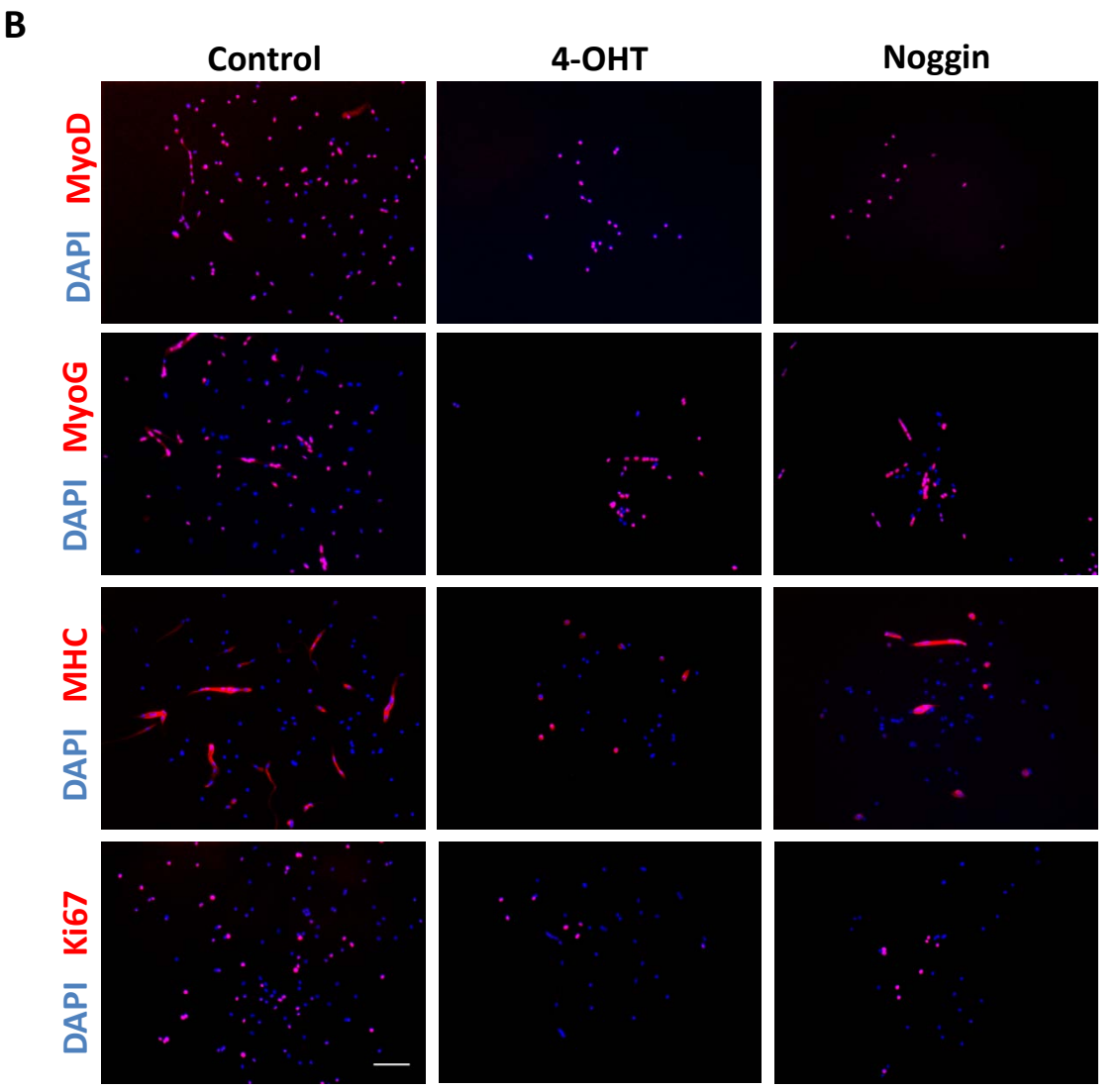

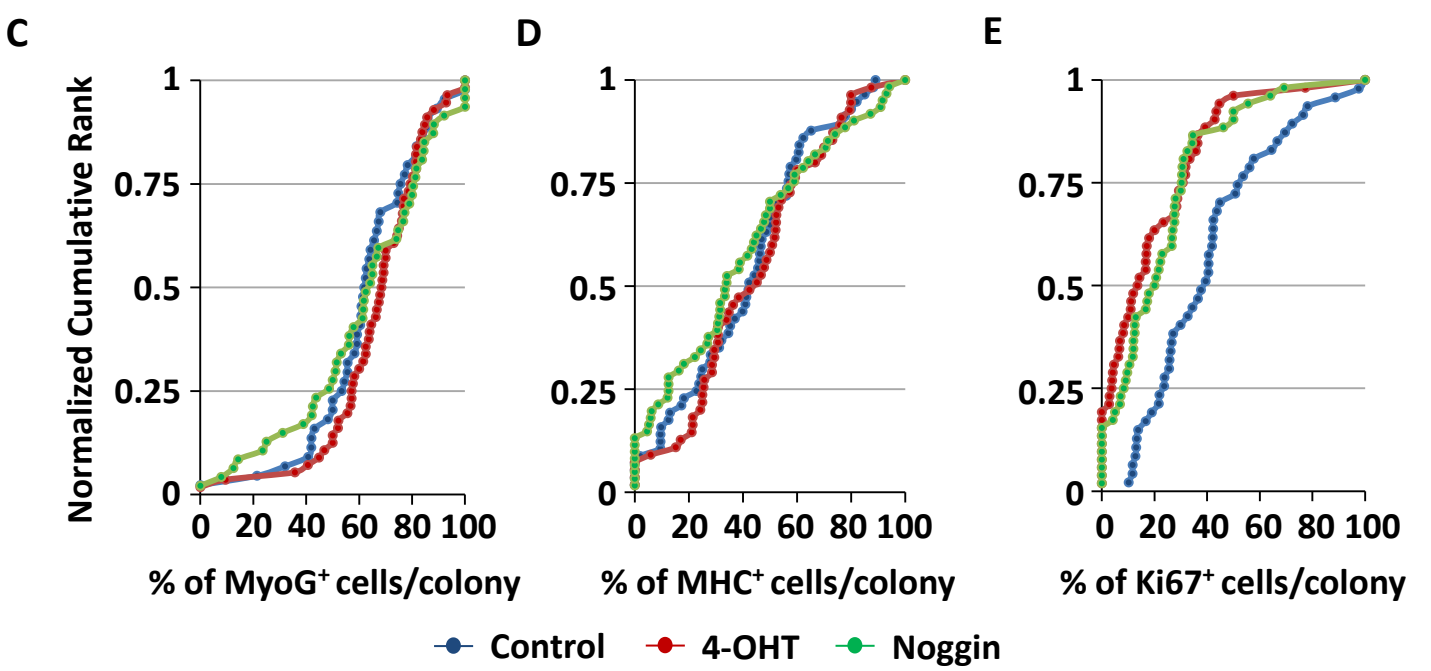

SUPPLEMENTARY METHODS

Generation of the conditional mouse line *Rosa26-LoxP-Stop-LoxP-huSMAD6-IRES-EGFP* (RS6)

For generation of the conditional SMAD6 overexpressing mouse line, the human *SMAD6* coding sequence present in the Mammalian Expression Clone EX-R0044-M02 (OmicsLink ™ ORF Expression Clones, Source BioScience) was inserted into the *pIRES2EGFP* vector (Clontech Laboratories). Cloning was enabled by inserting a *Nhe*I site into the *BstB*I site of the EX-R0044-M02 upstream of the *SMAD6* ORF *via* the synthetic oligonuctleotide 5'- GAA CTG CTA GCA GTT-3'. Next, the *Nhe*I/*Not*I *SMAD6*_IRESEGFP fragment was subcloned into the *pBigT* vector (Srinivas et al., 2001), which contained the *loxP*-flanked transcriptional STOP-codon combined with a *PGK-neomycin* cassette for positive selection of transfected embryonic stem (ES) cells. Finally, with the help of the enzymes *Asc*I, *Acc*I and *Pac*I, the floxedSTOP-*huSMAD6*-IRES-EGFP fragment was subcloned into the *Rosa26*-PA vector (this vector was modified before by inserting a *Fse*I site for linearization), which contained the homologous arms for recombination in the *ROSA26* locus and a *PGK-DTA* (Diptheria Toxin A) cassette for negative selection in ES cells (Srinivas et al., 2001; Soriano, 1999).

The *Fse*I-linearized floxedSTOP-*huSMAD6*-IRES-EGFP containing ROSA26 targeting vector was electroporated into V8.1 ES cells (129/FVB hybrid), G418 selected (400 µg/ml) and resulting clones characterized by Southern blot analyses using the 5' external probe "R26-5probeB" on *Eco*RV digested genomic ES cell DNA. The "R26-5probeB" probe was amplified from genomic DNA with the primers R26-5probeB_fwd: 5'-GTG GGG TCG ACT AGA TGA AGG-3'and R26-5probeB_rev: 5'-CTC ACG GGT ACG GGC CAT TCC-3'). Positive clones were injected into C57Bl/6 blastocysts and those implanted into foster mice.

Injection of ES cell clone #7 gave rise to chimeras, which transmitted the mutant *ROSA26* allele to the next generation by mating to C57Bl/6 mice. For genotyping, DNA was extracted from or mouse tails. PCR was used to determine the genotype of the *ROSA26* allele with the primers (Rosa-FA: 5'-AAA GTC GCT CTG AGT TGT TAT-3'; Rosa-RF: 5'-GGA GCG GGA GAA ATG GAT ATG-3', Rosa-SpliceAC: 5'-CAT CAA GGA AAC CCT GGA CTA CTG-3'). The amplified product of the mutant locus spans 249 base pairs (bp) while the product of the wildtype locus spans 585 bp.

AAV-production

The *Noggin* construct (AAV-*Nog*), was prepared by PCR amplification of chick cDNA (forward: 5'-ATG GAT CAT TCC CAG TGC CTT GTG AC-3' and reverse: 5'-CTA GCA GGA GCA CTT GCA CTC CGC GAT-3'), was subcloned into the *pCR2.1-TOPO* plasmid vector (TOPO Cloning, Invitrogen) and thereafter introduced into an AAV-2-based vector between the 2 inverted terminal repeats and under the control of the cytomegalovirus (CMV) promoter using the *Xho*I and *Eco*RI sites. The AAV2/1-*Noggin* (called AAV-*Nog*) was produced in human embryonic kidney 293 cells by the triple-transfection method using the calcium phosphate precipitation technique with both the *pAAV2* propeptide plasmid, the *pXX6* plasmid coding for the adenoviral sequences essential for AAV production, and the *pRepCAp* plasmid coding for AAV1. The virus was then purified by 2 cycles of cesium chloride gradient centrifugation and concentrated by dialysis. The final viral preparations were kept in PBS solution at -80°C. The particle titer (number of viral genomes) was determined by quantitative PCR.

Table S1. Oligonucleotides used for RT-qPCR

Gene	Primer sequence (5'→ 3')	Direction
Oligonucleotide primers used for mice		
Bmp1	TTTGATGGCTACGACAGCAC	Forward
	CTGTGGAGTGTGTCCTGGAA	Reverse
Bmp2	CATCACGAAGAAGCCGTGGA	Forward
	TGAGAAACTCGTCACTGGGG	Reverse
Bmp4	TCCATCACGAAGAACATCTGGA	Forward
	ATACGGTGGAAGCCCTGTTC	Reverse
Bmp5	AGGAATACACAAACAGGGATGC	Forward
	CCAGCAGATTTTACATTGATGC	Reverse
Bmp6	GGGATGGCAGGACTGGATCA	Forward
	ATGGTTTGGGGACGTACTCG	Reverse
Bmp7	AGCTTCGTCAACCTAGTGGAAC	Forward
	CTGGAGCACCTGATAGACTGTG	Reverse
Bmp13	AAGACTTACTCCATTGCCGAGA	Forward
	TCGTCCAGTCCTCTGTCTACAA	Reverse
Bmp14	ATGCTGACAGAAAGGGAGGTAA	Forward
	GCACTGATGTCAAACACGTACC	Reverse
Alk3	TGAGACAGCAGGACCAGTCA	Forward
	GATTCTGCCCTTGAACATGAGA	Reverse
Id1	GGTGGTACTTGGTCTGTCGG	Forward
	CCTTGCTCACTTTGCGGTTC	Reverse
Noggin	GAAGTTACAGATGTGGCTGTGG	Forward
	CACAGACTTGGATGGCTTACAC	Reverse
Gremlin1	AGCAAAAGGGTTTTCCTGAT	Forward
	AGTGGTCAGCATTTCACCCT	Reverse
Follistatin	CCTGCTGCTGCTACTCTG	Forward
	CTCGGTCCATGAGGTGCT	Reverse
p21	GTACTTCCTCTGCCCTGCTG	Forward
	GGGCACTTCAGGGTTTTCTC	Reverse
p57	CTGAAGGACCAGCCTCTCTC	Forward
	AAGAAGTCGTTCGCATTGGC	Reverse
Gapdh	TGACGTGCCGCCTGGAGAAA	Forward
	AGTGTAGCCCAAGATGCCCTTCAG	Reverse
Gapdh	GCATGGCCTTCCGTGTTC	Forward
	GGGTGGTCCAGGGTTTCTTACTC	Reverse
Oligonucleotide primers used for human cDNA insert in RS6 mice		
SMAD6	TACTCTCGGCTGTCTCCTCGC	Forward
	CAGTGGCTCGGCTTGGTGGCG	Reverse
Oligonucleotide primers used for chick		
Noggin	ATGGATCATTCCCAGTGCCTTG	Forward
	AGCTGCCCACTTTGACGTACCG	Reverse

SUPPLEMENTARY REFERENCES

Soriano, P., 1999. Generalized lacZ expression with the ROSA26 Cre reporter strain. Nat Genet 21, 70–71.

Srinivas, S., Watanabe, T., Lin, C.-S., William, C.M., Tanabe, Y., Jessell, T.M., Costantini, F., 2001. Cre reporter strains produced by targeted insertion of EYFP and ECFP into the ROSA26 locus. BMC Dev Biol 1, 4.